Standardized quality control workflow to evaluate the reproducibility and differentiation potential of human iPSCs into neurons

*Carol X.-Q. Chen [a], Narges Abdian [a], Gilles Maussion [a], Rhalena A. Thomas [a], Iveta Demirova [a], Eddie Cai [a], Mahdieh Tabatabaei [b], Lenore K. Beitel [a], Jason Karamchandani [b], Edward A. Fon [a], Thomas M. Durcan [a, *]*

[a] The Neuro's Early Drug Discovery Unit (EDDU), McGill University, 3801 University Street, Montreal, QC Canada H3A 2B4

[b] The Neuro's Clinical Biological Imaging and Genetic Repository (C-BIG), McGill University, 3801 University Street, Montreal, QC Canada H3A 2B4

***** Correspondence: Thomas M. Durcan, Email: thomas.durcan@mcgill.ca; Tel.: +1-514-398-6933.

Abstract

Induced pluripotent stem cells (iPSCs) derived from human somatic cells have created new opportunities to generate disease-relevant cells. Thus, as the use of patient-derived stem cells has become more widespread, having a workflow to monitor each line is critical. This ensures iPSCs pass a suite of quality control measures, promoting reproducibility across experiments and between labs. With this in mind, we established a four-step workflow to assess our newly generated iPSCs for variations and reproducibility relative to each other and iPSCs obtained from external sources. Our benchmarks for evaluating iPSCs include examining iPSC morphology and proliferation in two different media conditions (mTeSR1 and Essential 8) and evaluating their ability to differentiate into each of the three germ layers, with a particular focus on neurons. Genomic stability in the human iPSCs was analyzed by G-band karyotyping and a qPCR-based stability test, and cell-line identity authenticated by Short Tandem Repeat (STR) analysis. Using standardized dual SMAD inhibition methods, all iPSC lines gave rise to neural progenitors that could subsequently be differentiated into cortical neurons. Neural differentiation was analyzed qualitatively by immunocytochemistry and quantitatively by q-PCR for progenitor, neuronal, cortical and glial markers. Taken together, we present a standardized quality control workflow to evaluate variability and reproducibility across and between iPSCs.

Keywords: human induced pluripotent stem cells, quality control, genomic stability, trilineage differentiation, neural progenitor cells, cortical neurons

Abbreviations

5-FAM, 5-carboxyfluorescein; CV, crystal violet; E8, Essential 8 media; EB, embryoid body; ESC, embryonic stem cell; iPSC, induced pluripotent stem cell; HO 342, Hoechst 33342; ICC, immunocytochemistry; NE, neuroepithelial; NEAA, non-essential amino acids; NPC, neural progenitor cell; PBMC, peripheral blood mononuclear cells; PFA, paraformaldehyde; RT, room temperature; STR, short tandem repeat

Highlights

- Validation of culture conditions is critical in the expansion and maintenance of an iPSC line.
- Characterization of pluripotency and genomic stability ensures each line is free of defects at the DNA level, while maintaining its ability to be directed into any of the three germ layers.
- Forebrain cortical neurons can be generated from all iPSC line tested; however, the morphology and expression pattern of these neurons can vary from line to line.

1. Introduction

Human stem cells can give rise to any cell type when exposed to the appropriate developmental cues, holding enormous potential for tissue engineering, regenerative medicine and disease modeling. Since breakthrough studies over a decade ago demonstrated that human somatic cells could be reprogrammed into stem cells (Takahashi, Tanabe et al., 2007, Takahashi & Yamanaka, 2006), interest in applying human induced pluripotent stem cell (hiPSCs) approaches for disease modeling, drug screening and cell-based therapies has expanded dramatically. The growing number of iPSC lines and NIH-registered human embryonic stem cell (ESC) lines ensures that patient-derived pluripotent stem cells are now readily available to researchers, helping to accelerate our understanding of biology and disease and the development of therapies across disease areas (Daley, 2012). These developments underscore the need for iPSC quality standards that are sufficiently stringent to ensure that findings can be compared and results reproduced across laboratories (Dolgin, 2010).

Numerous studies on pluripotent ESCs and iPSCs have identified genomic instability as a critical parameter when monitoring the quality of cells for use in research or clinical applications. Common alternations that arise in the genome either during the iPSC reprogramming process (Lamm, Ben-David et al., 2016, Ruiz, Lopez-Contreras et al., 2015), from culture conditions (Bai, Ramirez et al., 2015) or from off-target CRISPR/Cas9 genome editing (Fu, Foden et al., 2013, Yang, Grishin et al., 2014) can include but are not limited to

(1) chromosomal/karyotypic abnormalities (Laurent, Ulitsky et al., 2011, Peterson, Westra et al., 2011, Taapken, Nisler et al., 2011) (reviewed in (Assou, Bouckenheimer et al., 2018, Rohani, Johnson et al., 2018), (2) copy number variations (CNVs), (3) small genomic insertions and deletions, or (4) single nucleotide variants (Martin, 2017). When present, these genomic abnormalities often alter the biological properties of hiPSC-derived models. Thus, before a given iPSC is used, it is tested for alternations at the genome level (Engle, Blaha et al., 2018, Rohani et al., 2018, Sullivan, Stacey et al., 2018).

In addition to assaying the genomic stability of an iPSC, it is more important than ever, that before an iPSC cell-line is utilized, its growth parameters are also optimized. Since the advent of iPSC technology, culture conditions have been designed to achieve formulations that are more standardized, helping to increase reproducibility between and within cell-lines. Two commonly used iPSC media are mTeSR1 (Ludwig, Levenstein et al., 2006) and Essential 8 (E8) (Chen, Gulbranson et al., 2011), both based on DMEM/F-12, for supporting the growth and maintenance of iPSCs. Yet, cell-lines can vary in their growth parameters depending on the media used, making it imperative that before working with any new cell-line, the optimal growth media and conditions for its maintenance and expansion be defined to reduce variations between lines (Chen et al., 2011, Hey, Saltokova et al., 2018, Akopian et al., 2010, Tano, Yasuda et al., 2014). Ensuring iPSC colonies maintain an undifferentiated morphology, determining the growth rate of each line, and assessing the pluripotency and differentiation potential of each line are essential quality control measures, to reduce variability and to increase reproducibility across different iPSCs.

Each benchmark for evaluating iPSCs has its own strengths and limitations in terms of sensitivity, costs, time and effort. Combining these standards, we propose a rigorous quality control workflow to evaluate the reproducibility of iPSCs to form human neurons. In this paper, we present our workflow combining these quality control (QC) assays to test for variability across ten newly generated hiPSC lines derived from healthy individuals, relative to existing commercial lines, and to evaluate the reproducibility and differentiation potential of human iPSCs into neurons. With these cell-lines, we established a workflow to monitor hiPSC morphology and proliferation in two different media (mTeSR1 and E8). Each iPSC was authenticated through Short Tandem Repeat (STR) profiling, to verify that each iPSC generated matched the parental cell from which it was reprogrammed. Genomic stability in the hiPSCs was analyzed by G-band karyotyping and qPCR-based profiling for genomic hotspot regions that are commonly altered during reprogramming (Assou et al., 2018, Attwood & Edel, 2019, Baker, Hirst et al., 2016). We also evaluated the pluripotency of our lines by examining their ability to form embryoid bodies (EBs) and to differentiate into each of the three germ layers, with a particular emphasis on their ability to form cortical neurons. We focused

on cortical neurons as methods to generate these neurons from iPSCs are well established and represent a cell type broadly studied across disease areas of the brain, from Alzheimer's disease to neurodevelopmental disorders (Brennand, Simone et al., 2011, Israel, Yuan et al., 2012). While all iPSC lines were capable of generating cortical neurons under standard differentiation protocols (Chambers, Fasano et al., 2009), line-to-line variability in the number of neurons formed, and their overall morphology was observed, highlighting the importance of deep phenotyping of cell lines before they are used in a given downstream application. Taken together, we present a straightforward multistep, QC workflow (**Figure 1**) to evaluate variations and reproducibility between our iPSCs in differentiating human neurons for downstream applications.

2. Materials and methods

2.1. Cell lines

The following lines were used: H9 hESC (Wicell), NCRM1 (NIH), KYOU-DXR0109B (ATCC), AIW002-02, AJC001-5, AJG001-C4 (same donor but reprogrammed using different methods or from different cell types), AJD002-3, TD03 (same donor but reprogramming with different methods), TD2, TD10, TD22, 3448 and 3450. The complete profiles of the iPSCs are listed in **Table 1**. The use of iPSCs and stem cells in this research is approved by the McGill University Health Centre Research Ethics Board (DURCAN_IPSC / 2019-5374).

2.2. iPSC reprogramming

PBMCs and skin fibroblast cells were obtained through the C-BIG Repository at the Montreal Neurological Institute (The Neuro). For iPSC reprogramming, AIW002-02, AJC001-5 and AJD002-3 were generated using the CytoTune™-iPS 2.0 Sendai Reprogramming Kit (iPSQuebec Platform, Laval University) and TD02, TD03, TD10 and TD22 through episomal reprogramming (Axol Biosciences, UK). AJG001-C4, 3448 and 3450 were generated in house by episomal reprogramming. For "*in house*" reprogramming, PBMCs were cultured in Stemline II Hematopoietic Stem Cell Expansion Medium (Sigma; S0192) supplemented with stem cell factor (100 ng/ml, Peprotech; 300-07), interleukin-3 (10 ng/ml, Peprotech; AF-200-03), erythropoietin (2 U/ml Peprotech; 100-64), insulin growth factor-1 (20 ng/ml Peprotech; 100-11), dexamethasone (1 mM, Sigma; D4902) and 1-thioglycerol (0.2 mM Sigma; M6145). After 6 days of culture, 2~3 x10^6 cells were nucleofected with episomal plasmids (pEV-OCT4-2A-SOX2, pEV-MYC, pEV-KLF4, and pEV-BC-XL, a generous gift from Dr. XB Zhang, Loma Linda University). The transfected PBMCs were plated on mitomycin C-treated mouse embryonic fibroblasts cultured in KnockOut DMEM/F12 (Gibco; 112660-012) with 1x L-

glutamine (Gibco; 25030-081), 1x penicillin/streptomycin (Gibco; 15140-122), 1x non-essential amino acids (NEAA) solution (Gibco; 11140-050), fibroblast growth factor 2 (50 ng/ml Peprotech;100-18B), 1x Insulin-Transferrin-Selenium (ITS Gibco; 41400-045), and 2-phospho-L-ascorbic acid (50 mg/ml, Sigma; 49752). On day 4, the culture was refreshed with 2 ml of the above medium. When colonies displayed iPSC morphology (between day 6-8 post-transfection), cells were fed with mTeSR1 medium (Stemcell Technologies, 85850, 85857) supplemented with sodium butyrate (0.25 mM, Sigma; B5887) every 2 days until day 14. Colonies were picked on day 14-16 by manual colony picking and cultured on Matrigel-coated dishes every 5–7 days for five passages when they were cryopreserved for further testing and profiling (Wen, Zhang et al., 2016).

2.3. Culture conditions for iPSCs

iPSCs were cultured and expanded on Matrigel (Corning, 354277)-coated plates in either mTeSR1 or E8 (ThermoFisher Scientific, A1517001) media, attaining a confluency of 10-15% one day after cell passage, with daily media changes until cells were next ready to passage again. Cells were maintained at 37°C with 5% CO_2 and split when cells reached 70-80% confluency (within 5-7 days of seeding). iPSCs were manually groomed by removing any colonies with irregular borders, spontaneous differentiation or transparent centers, prior to splitting. Cells were passaged by incubation in Gentle Cell Dissociation media (Stemcell Technologies, 07174) for 4 minutes at 37°C to obtain single cells or RT for 6 minutes to obtain small aggregates of colonies. The following cell densities were used: 2×10^4 cells/well in 24 well plates for immunocytochemistry; 2×10^4/60 mm dish for daily morphology imaging; 2×10^5/well in 6 well plates for EB formation.

2.4. Crystal violet assay

For this assay, 4000 cells/well were plated in Matrigel-coated 96-well plates with mTeSR1 or E8 media. After 2, 4 or 6 days in culture, plates were rinsed with PBS to remove non-attached cells and fixed with 3.7% PFA for 5 minutes, before being stained with 0.05% crystal violet (CV, Sigma,46364) diluted in water for 30 minutes. The CV dye was thoroughly washed away with distilled water, and the plates dried at RT. Once dried, the plates were imaged and quantification performed (Feoktistova, Geserick et al., 2016) by adding 100 µl of methanol (Fisher Chemical, 32435K7) to the wells to solubilize the CV, followed by measurement of the O.D. at 540 nm (OD540) with an EnSpire Multimode Plate Reader (Perkin Elmer).

2.5. RNA isolation, cDNA synthesis, and qPCR analysis

RNA was purified with a NucleoSpin RNA kit (Takara) according to the manufacturer's instructions. cDNA was generated using the iScript Reverse Transcription Supermix (BioRad). Quantitative real-time PCR was performed on the QuantStudio 5 Real-Time PCR System (Applied Biosystems) using the primers listed in **Supplementary Table S2**. Raw data was processed using a custom Python script available at https://github.com/RhalenaThomas/Auto-qPCR/tree/master/auto-q-pcr-command_line The cycle threshold (CT) values for technical triplicates were tested for outliers. Relative gene expression was calculated by using the Comparative CT Method (ΔΔCT method), where the endogenous controls were GADPH or ACTB expression, the reference sample varies by experiment and is indicated in each plot.

2.5. Short Tandem Repeat (STR) analysis

All newly generated iPSCs were authenticated through STR analysis with the GenePrint® 10 System (Promega, B9510) at The Centre for Applied Genomics, the Hospital for Sick Children, Toronto. Briefly, genomic DNA from the iPSCs or the source material for the iPSCs, which in this case was PBMCs, was extracted with a Genomic DNA Mini Kit (Blood/Cultured Cell) (Geneaid, GB100). Ten ng of genomic DNA was mixed with GenePrint® 10 primer pair mix to permit co-amplification and detection of ten human loci, including all ASN-0002-2011 loci (TH01, TPOX, vWA, CSF1PO, D16S539, D7S820, D13S317, D5S818) plus Amelogenin for sex determination and one mouse locus D21S11. These loci collectively provide a genetic profile with a random match probability of 1 in 2.92×10^{9}.

2.6 Genome stability test and karyotyping

Genomic DNA was extracted with the Genomic DNA Mini Kit. Genomic stability was detected with the hPSC Genetic Analysis Kit (Stemcell, 07550) according to the manufacturer's instructions. Briefly, 5 ng of genomic DNA was mixed with a ROX reference dye and double-quenched probes tagged with 5-FAM. The probes represented the eight most common karyotypic abnormalities reported in hiPSC: chr 1q, chr 8q, chr 10p, chr 12p, chr 17q, chr 18q, chr 20q or chr Xp. Sample-probe mixes were analyzed on a QuantStudio 5 Real-Time PCR System (ThermoFisher Scientific). Copy numbers were analyzed using the ΔΔCt method. The results were normalized to the copy number of a control region in chr 4p (Baker et al., 2016). For G-band karyotyping, iPSCs were cultured for 72h until they attained a 50-60% confluency, then shipped live to the Wicell Cytogenetics Core (instructions provided by WiCell).

2.7. Three Germ Layer Differentiation Test

To form EBs, two wells of a 6 well plate containing 80-90% confluent iPSCs were dissociated into small clumps and cultured into low-attachment tissue plates in their preferred iPSC maintenance media (based on findings from CV assays in **2.4**.). On day 7, EBs were transferred to Matrigel-coated plates and left to spontaneously differentiate for 14 days in DMEM media (Wisent, 319-005-CL) containing 20% FBS (Gibco, 10091), 1% NEAA solution (Wisent, 321-011-EL), 0.1 mM 2-mercaptoethanol (Gibco, 31350010) before fixation and immunocytochemistry.

To differentiate iPSC into each of the three germ layers, iPSCs were passaged and dissociated as described above for EB generation into single cells and cultured on Matrigel-coated plates with the STEMdiff Trilineage differentiation kit (used according to the manufacturer's instructions, Stemcell Technologies, 05230). Cells were harvested at the indicated day for gene expression by q-PCR.

2.8. Immunocytochemistry analysis

Cells were fixed in 4% PFA/PBS at RT for 20 minutes, permeabilized with 0.2% Triton X-100/PBS for 10 min at RT, then blocked in 5% donkey serum, 1% BSA and 0.05% Triton X-100/ PBS for 2h. Cells were incubated with primary antibodies in blocking buffer overnight at 4 °C. Secondary antibodies were applied for 2h at RT, followed by Hoechst 33342 nucleic acid counterstain for 5 minutes. Immunocytochemistry images were acquired using the automated Evos FL-Auto2 imaging system (ThermoFisher Scientific). Antibodies used for staining were listed in **Supplemental Table S1**. Images were quantified using custom ImageJ macros. The analysis scripts are available at https://github.com/neuroeddu/CellQ. The thresholds were determined visually by comparing five randomly sampled images.

2.9. Cortical neuronal differentiation

Differentiation into cortical neurons was based on a protocol for EB formation combined with dual inhibition of SMAD (Chambers et al., 2009, Zhang, Wernig et al., 2001) with some additional modifications. Briefly, each iPSC line was cultured in its preferred media for 5-7 days, then dissociated into single cells to form EBs. The EBs were grown in a low-attachment plate for one week in DMEM/F12 supplemented with N2 and B27, in the presence of 10 μM SB431542, and 2μM DMH1. On day 7, EBs were transferred to polyornithine- and laminin-coated plates to form rosettes in the same media. On day 14, rosettes were selected semi–manually and cultured as a monolayer on polyornithine and laminin-coated plates to generate NPCs in DMEM/F12 supplemented with N2 and B27. NPCs were passaged at a 1:3 dilution every 5-7 days. Immunocytochemistry and q-PCR analysis of NPC were conducted at day 25.

NPCs were next cultured in neurobasal medium, supplemented with N2 and B27, in the presence of 1 µg/ml laminin, 500 µM db-cAMP, 20 ng/ml BDNF, 20 ng/ml GDNF, 200 µM ascorbic acid, 100 nM Compound A and 1 ng/ml TGF-β for differentiation into neurons. Immunocytochemistry and q-PCR analysis of cortical neurons were conducted at day 56.

2.10. Data visualization and statistical analysis

All data visualization plots were created in R using the ggplot2 graphical package. For RNA quantification the standard deviation (SD) values were calculated in Python. For better visualization of the RNA quantification the values were log transformed, and the SD was equivalently scaled. For image analysis SD values were calculated in R. For all plot variation is presented as mean ±SD. A minimum of two independent replicates for each experiment were performed. For calculating the difference in gene expression between two medias, two-tailed students t-tests were performed using the t.test function in R, individual cell lines were considered biological replicates (n=6 mTeSR1, n=5 E8).

3. Results

3.1. Validation of hiPSC culture conditions

To work with any iPSC line, it is critical to first establish the optimal growth conditions for that cell-line. As a first step in the workflow, and as part of the initial tests for our newly reprogrammed iPSCs, we grew all our newly generated cell-lines side by side in two distinct maintenance media: mTeSR1 or E8. Additional commercial iPSC lines (NCRM1-NIH and KYOU-DXR0109B-ATCC) were also grown in both media for direct comparison with our "*in house*" control lines (the profiles of each cell line are provided in **Table 1**). Cells were seeded at an identical confluency and cultured in Matrigel-coated plates in either mTeSR1 or E8 media. We first examined cells 24h after passaging for differences in their overall attachment, spontaneous differentiation and morphology as they grew and expanded. All iPSC lines attached onto Matrigel-coated plates and demonstrated similar morphology when maintained in either media condition. The condensed, round, diffuse and irregularly shape associated with iPSC colonies was observed with all cell lines. The colonies were smooth-edged, with tightly packed cells by phase contrast imaging (**Fig. 2A and 3A**). Rare incidences of spontaneous differentiation, in which the cells lost their pluripotency, could be observed in both media conditions and across the different cell-lines.

Although morphology is one indicator of the quality of cultured iPSCs, growth properties can vary from line to line, which can be influenced by the maintenance media used to culture the iPSCs. To detect differences in growth rates and adherence of cells over time, cells were

fixed and stained with crystal violet (CV). CV staining (Feoktistova et al., 2016) is directly proportional to cell biomass and provides a quick and straightforward method to quantify the proliferation of each cell line at different time points. **Fig. 2B and S1** demonstrate that the growth rate of all cell-lines in each media condition was comparable at day 2. By day 4, three lines were observed to be growing at a faster rate in E8 (AJD002-3, 3450 and TD10; **Fig. 2C and S1**) and exhibited reduced growth and proliferation when maintained in mTeSR1. By day 6, the difference in growth rates was further pronounced for these lines, with 3448 and TD22 also demonstrating a preference for E8. Of note, the proliferation rate for AJC001-C4 was the slowest across the lines, growing at a comparable rate in both media (**Fig. 2C and S1**). For our panel of iPSCs, variations in the growth rate between certain iPSCs was observed depending on the media conditions. Thus, in the rest of our assays, the cells were grown in their preferred media (**Table 1**). Taken together, daily morphological observations coupled with a CV assay, enable a rapid assessment of the growth conditions for a given cell-line, ensuring that each iPSC is cultured in its optimal media for growth and expansion.

3.2. Characterization of pluripotency of hiPSCs

Next, we examined the pluripotency characteristics of each iPSC line in their preferred growth media (mTeSR1 or E8), as determined by the CV assays (**Fig. 2**). All iPSC lines tested expressed the pluripotency markers SSEA-4, OCT3/4, NANOG and Tra-1-60R, in the same manner as the H9 ESC cell-line. The cell lines displayed no differences in the fluorescence intensity of these markers (**Fig. 3A**). Notably, we found that over 90% of cells were OCT3/4 or SSEA-4 positive, demonstrating that the cells were maintained in a state of pluripotency with rare spontaneous differentiation (**Fig. 3B**). iPSCs were not only morphologically similar to each other and to ESCs; but were also similar at a transcriptional level for common pluripotency markers (OCT3/4, SOX2, NANOG). (Maherali, Sridharan et al., 2007, Mikkelsen, Hanna et al., 2008, Okita, Ichisaka et al., 2007, Takahashi et al., 2007, Wernig, Meissner et al., 2007). To examine the transcriptional profile of our lines, the embryonic stem cell, H9 was used as a reference line to normalize the expression of pluripotency genes relative to each of the control iPSC lines (Allegrucci & Young, 2007). The expression of Yamanaka factors (OCT3/4, SOX2, KlF4 and c-MYC) and two other widely used pluripotent markers, NANOG and ZFP42 (Rex1) (Son, Choi et al., 2013) were analyzed by q-PCR (**Fig. 3C**). We found that all iPSC lines expressed each of pluripotency genes, and expression levels for each gene was comparable to those observed for the H9 ESC cell-line. However, variations in expression of the genes was observed between the lines. We found that NCRM1 and KYOU-DXR0109B, two commercial control lines with high passage numbers, expressed relatively high levels of NANOG, SOX2 and ZFP42 when compared to

H9, suggesting that prolonged periods of proliferation and self-renewal may stabilize and perpetuate the genome of the hiPSC in a pluripotent state. Given our iPSCs are at an earlier passage number, these levels were lower, consistent with previous studies showing that hESC-specific genes (Lowry, Richter et al., 2008) are expressed at lower levels in early passage iPSCs compared to ESCs and late passage iPSC (Chin, Mason et al., 2009).

3.3. STR and genomic stability analysis of hiPSCs

The risk of cell misidentification and cross-contamination has plagued cell research, (Cabrera, Cobo et al., 2006, Chatterjee, 2007). In addition, hiPSCs which are generated and grown on a layer of mouse embryonic fibroblasts (MEF) feeder cells are often at risk of cross-contamination with these non-human rodent somatic cells (Yaffe, Noggle et al., 2016). For this reason, we conducted STR analysis for iPSC authentication. Our analysis demonstrated that the STR profile for each iPSC tested matched the parental cell-line from which it was reprogrammed, and no rodent contamination was detected with any of our iPSCs. As both AJD002-3 and TD03 were generated from the same donor, they displayed identical STR profiles relative to each other, and to somatic cells obtained from this donor (PBMC sample #3059) (**Table 2**).

Numerous studies have demonstrated that ESCs and iPSCs accumulate genomic alterations and mutations though reprogramming processes and long-term culture. At the genome level these changes can include copy number variations, trisomy's, small genomic insertions and deletions, and single nucleotide variants. In order to assess chromosomal instability of the iPSC lines, G-band karyotyping was performed. Our analysis showed the majority of the iPSCs tested had a normal 46, XY or 46, XX karyotype (**Fig. 4A and S2**). However, we did detect a chromosomal anomaly with the TD10 line, which contained a translocation between the long (q) arm of chromosome X and the short (p) arm of chromosome 2. These abnormalities were confirmed to be a direct result of reprogramming, as follow-up G-band analysis of the parental PBMCs showed a normal karyotype (data not shown). This confirms that the chromosomal rearrangement in TD10 likely occurred during the reprogramming process and disqualifies this line from further use.

Although karyotyping by G-banding reveals both numerical and structural aberrations within chromosomes, the limited resolution of this method means we can only detect chromosomal aberrations greater than 5 Mb in size (Amps et al., 2011, Lund, Narva et al., 2012, Taapken et al., 2011). To test for commonly occurring genomic alterations, we used a qPCR-based genetic analysis kit to detect minimal critical hotspot regions within the genome that are frequently targeted during the reprogramming process, and which often confer selective

growth advantages (Hussein, Batada et al., 2011, Narva, Autio et al., 2010). Using this assay, we did not detect any increase or decrease in copy number outside the confidence interval (1.8 to 2.2) indicating there are no abnormalities in any of the hotspot zones on chr 1q, chr 8q, chr 10p, chr 12p, chr 17q, chr 18q, chr 20q and chr Xp with our "*in house*" iPSCs, which cover the majority of the reported abnormalities (**Fig. 4B**) (Ben-David, Mayshar et al., 2011, Draper, Smith et al., 2004, Inzunza, Sahlen et al., 2004, Lefort, Feyeux et al., 2008, Sareen, McMillan et al., 2009). However, there was one exception where we did note a moderate increase in the copy number for chr 20q in our TD03 line (**Fig. 4B, indicated with #**). However, with both the commercial lines, NCRM1 and KYOU-DXR0109, an amplification in copy number on chromosome 20q was detected (**Fig. 4B, indicated with an arrow**), suggesting that this instability expanded with extensive cell passage. Thus, it is imperative that, when working with any iPSC line, it is first profiled for the presence of genomic instability at common sites, which might otherwise affect its growth and differentiation.

3.4. Differentiation of hiPSCs into three germ layers

One of the hallmark features of iPSCs is their pluripotency, an ability to differentiate into nearly any cell type of the three germ layers when provided the right developmental cues. To characterize the functional pluripotency of our newly generated iPSCs relative to the commercial lines, we tested their ability to form EBs in which cells spontaneously differentiated into each of the three embryonic germ layers. After one week, iPSCs successfully formed EBs and no discernible differences in the relative size and total number of EBs formed was detected between lines. Following the formation of EBs in defined media, they were plated onto Matrigel-coated dishes in the presence of serum-containing media and cultured for 2 weeks. All iPSCs tested could differentiate into each of the three germ layers, as shown by positive immunostaining for the ectoderm marker PAX6, the mesoderm marker SMA and the endoderm marker Vimentin (**Fig. 5A**).

In parallel to our imaging analysis, we also took advantage of a q-PCR based assay to permit a faster, more quantitative assessment of functional pluripotency. Through this approach, we can quantify the *in vitro* differentiation potential of our hiPSCs by measuring the relative expression of key genes that represent each of the three specific lineages. We used the H9 ESC as our control to compare the expression of three germ layer genes in the iPSC lines. As shown in **Fig. 5B**, cells differentiated from iPSCs into each of the three lineage layers expressed either the ectodermal markers PAX6 and NCAM, the mesodermal marker MIXL1 or the endodermal marker Vimentin, depending on their given lineage. However, while all the lines expressed each of these markers, variations were observed between lines, potentially indicating differing capabilities for each line to generate the different germ layers. For instance,

3450 expressed high levels of both Pax6 and MIXL1, while also expressing the lowest levels for Vimentin, indicating this line is likely best used to generate cells of an ectodermal or mesodermal lineage. In contrast, TD10 expressed all the lineage markers at relatively high levels, indicating that the presence of the karyotypic abnormality had no effect on its ability to differentiate and form each of the three germ layers. ICC staining and q-PCR findings highlight that all iPSCs were capable of differentiation into each of the three germ layers. However, based on the expression analysis, the abilities of iPSC to generate different cell types were variable, highlighting the need to choose iPSC lines carefully based on the cell types that will be generated for downstream applications.

3.5. Differentiation of iPSCs into cortical neurons

Following our trilineage analysis, we narrowed our focus to examine the ability of our iPSCs to form one specific cell type from the ectodermal lineage, cortical neurons. To generate cortical neurons, we used a previously published dual SMAD inhibition protocol with some modifications (Chambers et al., 2009, Zhang et al., 2001). **Fig. 6A** shows the timeline schematic for the protocol, in which iPSCs were differentiated into neurons over 56 days. EBs were formed by dissociating iPSCs at day 0. After 14 days of neural induction, columnar neuroepithelium cells and typical neural tube-like rosettes appeared with all iPSC lines. Rosettes were dissociated and expanded into neural progenitor cells (NPCs). All the characterization of NPCs was performed at day 25. We found that all iPSC lines could generate NPCs, as demonstrated by positive immunostaining for the neural progenitor markers Nestin, SOX1, and still maintained an ability to proliferate, as shown by the presence of the cell proliferation marker Ki67 (**Fig. S3**). Based on the quantification of immunostaining, approximately 60-80% of cells from the iPSCs tested were Nestin-positive. In contrast, 10-25% of the cells for each line expressed SOX1 or Ki67 (**Fig. S3B**). The pluripotency markers POU1F5 and NANOG, the mesodermal marker MIXL1 and the endodermal marker AFP were expressed at low levels which was to be expected given the cell type being generated is an ectodermal lineage (**Fig. S4A and S4B**). The expression of the NPC marker Nestin was further confirmed by q-PCR (**Fig. S4C**). NPCs also expressed dorsal forebrain progenitor markers SLC1A3 and PAX6, and the ventral forebrain progenitor marker ASCL1 (**Fig. S4C**), which confirms that the iPSCs tested can differentiate into NPCs (Chambers et al., 2009).

NPCs generated from each line were subsequently differentiated into cortical neurons that we analyzed through a combination of qPCR and ICC analysis (**Fig. 6A**). qPCR results confirmed high expression levels of the neuronal markers MAP2, NCAM1 and Tuj (TUBB3) in neurons at day 56 differentiation (**Fig.6B**). Furthermore, upper layer (SATB2) or lower layer (FOXP1) cerebral cortex markers were detected in neurons (**Fig. 6C**). However, the

expression level of these markers exhibited line to line variation. Intriguingly, we compared expression levels in the neurons derived from iPSCs lines maintained in mTeSR1 to neurons from iPSC maintained in E8 and found that levels of these markers was significantly higher for neurons derived from iPSCs maintained in mTeSR1 ($p= 0.0349$ MAP2; $p=0.017$ NCAM1; $p= 0.018$ TUBB3; $p = 0.008$ FOXP1 and $p = 0.010$ SATB2) (**Fig. S5**). The higher expression levels of these markers implies that the iPSC maintenance media may influence the differentiation potential of iPSCs, and in this case specifically, into cortical neurons, meriting further investigation. Based on the quantification of the immunostained neurons, approximately 80-90% of cells expressed MAP2 and 60-80% of cells were Tuj1-positive neurons, varying from line to line (**Fig. 7**). In contrast, the expression of the cortical neuron markers Brn2 or Tbr1 was much more variable (5-30%) across cell-lines (**Fig. 7**). Taken together, the iPSCs tested can generate neurons, although variations in morphology and expression of neuronal or cortical region markers does vary across lines. Thus, such variables may similarly impact iPSC differentiation into other cell types making it imperative that before any studies, an iPSC is comprehensively phenotyped to obtain a baseline on its cellular characteristics.

4. Discussion

The routine utilization of iPSCs requires a constant supply of pluripotent, well characterized and quality-controlled cell stocks. Here, we established a workflow to monitor the morphology and proliferation of iPSCs in two different media (mTeSR1 and E8). In parallel, we evaluated the genomic stability, pluripotency and differentiation potential of our lines. Based on these parameters, we can evaluate the suitability of iPSCs for use in further applications. By focusing on cortical neurons, we can also better predict how variable cell-lines are in their ability to generate cortical neurons with the same methods while understanding how the neurons generated might differ from line to line, or from batch to batch within the same line.

Culture conditions can affect the stability, growth rate and pluripotency of iPSCs (Bai et al., 2015, Lamm et al., 2016, Martin, 2017, Ruiz et al., 2015). Today, commercially available medium, for example, mTeSR1 and E8 are widely used to culture iPSCs (Chen et al., 2011, Hey et al., 2018, Akopian et al., 2010, Ludwig et al., 2006, Tano et al., 2014). While many lines grow in both media at comparable rates, some cells have a preference for one or the other. With our panel of iPSCs, five cell lines grew faster in E8 (**Fig. 2B, 2C and S1**). Why certain lines might proliferate faster in one media versus another is still not clear, but it has been demonstrated previously that the reduced composition of E8 (8 factors) often elicits a faster growth rate (Tano et al., 2014). Yet, what is less clear is why the cells grew well in E8, while their growth rate appeared to stall in mTeSR1, which was observed for both the 3450

and TD10 cell-lines. Interestingly, we found that cell lines derived from the same donor (AJC001-5 and AIW002-02), but from distinct somatic cells (PBMC vs skin fibroblasts), tended to grow at comparable rates in either media type. Among lines generated from the same donor's PBMCs (AJD002-3 and TD03), the reprogramming methods (Sendai CytoTune vs. episomal) also did not appear to affect the media in which they preferred to grow in. Thus, before working with any iPSC it is imperative that culture conditions are optimized. Moreover, if a line appears to have slower growth with one media type, it is recommended to test other media conditions as certain factors in the media may impact the overall growth rate for a given line.

Expression of pluripotency-associated markers is an important quality criteria for any iPSC line, otherwise the iPSCs cannot be differentiated into a cell type of interest. All iPSC lines in our study expressed the commonly studied pluripotency markers (SSEA-4, OCT3/4, NANOG and TRA-1-60R) (**Fig. 3A and B**). We did find that OCT3/4 expression level was approximately 15 times higher than that of SOX2 (**Table S3**), consistent with previous studies, showing that this OCT3/4 high, SOX2 low stoichiometry is important not only in the early phase of facilitating cells reaching a fully reprogrammed state, but also in the late phase of iPSC maturation and maintaining pluripotency (O'Malley, Skylaki et al., 2013, Papapetrou, Tomishima et al., 2009, Yamaguchi, Hirano et al., 2011). Further evidence has also demonstrated that OCT3/4 downregulates the downstream gene expression of NANOG, SPP1/ OPN, SOX2, FBXO15, OTX2, and ZFP42/REX1 (Matoba, Niwa et al., 2006). The expression levels of NANOG, ZFP42 and c-MYC in our study were approximately 50 times lower than that of OCT3/4, which is consistent with previous results from sc-RNA-seq iPSC dataset (Daniszewski, Nguyen et al., 2018, Nguyen, Lukowski et al., 2018). Interestingly, NCRM1 and KYOU-DXR0109B, two commercial control lines with high passage number (>30 passages), express relatively high level of NANOG, SOX2 and ZFP42 and reduced levels of OCT3/4, suggesting that extended passaging enhances pluripotency gene expression (Koehler, Tropel et al., 2011).

Numerous studies have demonstrated that both ESCs and iPSCs accumulate genomic instability during long-term culturing, and often is the primary reason why clinical therapies from stem cells were not administered to patients (Mandai, Watanabe et al., 2017). G-banding is the most widely used technique for genetic evaluation of iPSCs (Taapken et al., 2011) and upon karyotyping, the majority of iPSCs we tested maintained a normal karyotype (**Fig. 4A and S2**). However, we were able to detect a genomic anomaly in one of our control lines, TD10 which presented with a translocation between the long (q) arm of chromosome X and the short (p) arm of chromosome 2. Yet, when compared to other cell types, this line appears within the normal range perfectly normal for all other parameters, highlighting how important it is to assess every line for genomic instabilities that might impact findings in downstream applications. To overcome limited resolution of G-binding assay, we also use a qPCR-based

genetic analysis which covers the majority of reported abnormalities, although for our lines we did not detect any abnormalities (**Fig. 4B**) (Ben-David et al., 2011, Draper et al., 2004, Inzunza et al., 2004, Lefort et al., 2008, Sareen et al., 2009). However, with the two commercial lines, NCRM1 and KYOU-DXR0109, an amplification in copy number on chromosome 20q was detected (**Fig. 4B, labeled with an arrow**). This region is enriched with genes associated with pluripotency and anti-apoptosis, including DNA methyl-transferase 3B (DNMT3B), inhibitor of DNA binding 1 (ID1), and BCL2-like1 (BCL2L1) (Lefort et al., 2008, Scotto, Narayan et al., 2008). We also detected a slight increase in copy number for chr8q in NCRM1, which is an abnormality acquired during prolonged periods in culture as previously reported (Taapken et al., 2011), suggesting rigorous quality control is needed with these lines, as it is likely that with increasing cell passage, this instability has expanded. These findings strongly imply that lines must be tested for genomic instabilities that can arise through reprogramming and prolonged cell passage. Otherwise, it can be difficult to interpret findings as one line may grow better or differentiate better due to one of these hotspot mutation.

A core feature of hiPSCs is their ability to differentiate into nearly any cell type of the three germ layers. All the iPSCs tested in our study had the potential to differentiate into each of the three germ layers, as shown by positive immunostaining for the ectoderm, mesoderm and endoderm markers PAX6, SMA and Vimentin, respectively (**Fig. 5A**), as previous reported (Itskovitz-Eldor, Schuldiner et al., 2000). We also took advantage of a q-PCR based assay to enable faster, more quantitative assessment of functional pluripotency, relative to the image-based approach of the EB trilineage test. From this test, all the iPSCs expressed markers for each of the three germ layers, albeit at differing levels, with some lines expressing higher levels of one or more markers compared to each other (**Fig. 5B**). Nevertheless, depending on the line itself, some consideration needs to be given as to whether it is the optimal line required to generate a particular cell type of interest. Moving beyond a broad trilineage test, we also tested our lines for their ability to form one specific cell type of interest: cortical neurons. NPCs generated from each line were differentiated into cortical neurons; with 80-90% of cells expressing the neuronal marker MAP2 and 60-80% of cells staining positive for Tuj1, although this varied from line to line. Consistent with published findings, these neurons also demonstrated a cortical layer identity, albeit one that varied across lines. Based on ICC and q-PCR results, ~5-25% of neurons from the iPSCs tested expressed Brn2, a marker of upper layer L2-L5 cortical neurons and previously shown to regulate general migration mechanism (Sugitani, Nakai et al., 2002). The upper layer identity has been further demonstrated by elevated expression of SATB2, another transcription factor found in cortical L2-L5 neurons (Britanova, de Juan Romero et al., 2008). Further evidence of this variability in neuronal identity was shown for the post-mitotic corticothalamic neuronal marker TBR1, which could be found in anywhere from 5-30% of neurons. The expression of Foxp1 in cortical neurons also

supported the lower layer feature (Ferland, Cherry et al., 2003). Taken together, our findings indicate that expression levels for these markers was highly variable across iPSCs. The variability did not appear to come from the differentiation protocol, as all the iPSCs were differentiated under the same conditions. This variability may not simply be a direct result of distinct genetic background differences, since variations in differentiation were also detected between AIW002-02, AJC001-5 and AJG001-C4 which share the same genetic background. Intriguingly, the iPSCs maintained in mTeSR1, expressed FOXP1 and SATB2 at levels much higher than those maintained in E8, potentially indicating that the conditions we culture the cells might impact their ability to form defined types of neurons, an area which warrants further study. If media conditions did in fact affect the differentiation potential of a given cell, this would make it even more imperative that we accurately define the optimal conditions for growing and maintaining an IPSC line to be used in making our cell type of interest.

5. Conclusions

Reprogramming of somatic cells into iPSCs opens up the possibility of modeling human diseases and developing new therapeutics. Thus, in this study, we established a workflow to monitor the morphology and proliferation of newly generated iPSCs in two different media (mTeSR1 and E8). We also performed a comprehensive phenotyping of the iPSC lines through profiling STR, genome stability, pluripotency and the ability to form the three germ layers, with a focus on cortical neurons of the ectodermal lineage. From these studies, all iPSCs share common hallmarks, yet can vary in their growth rate or ability to differentiate into other cell types. Given our findings, it is imperative that each iPSC lines is evaluated thoroughly before using it in downstream applications.

Author Contributions

CXQC and TMD designed the study and worked with JK and MT to implement stem cell ethics and to provide PBMCs for reprogramming and to assist with biobanking of completed iPSCs. CXQC and NA performed the experiments. GM, IV and EC wrote Python for q-PCR analysis. RAT and EC wrote the Macros for ICC quantification. RAT and EC wrote R scripts for graphs and statistics. CXQC, NA, RAT and TMD analyzed the data. CXQC, NA, LB, EAF and TMD wrote the paper with input from all authors. All authors approve the content in this manuscript.

DECLARATION OF COMPETING INTEREST

The authors declare that they have no known competing financial interests or personal relationships that could have appeared to influence the work reported in this paper.

Acknowledgments

We thank Drs. Mark Aurousseau and Wolfgang Reintsch for automated image acquisition, Angela Nauleau-Javaudin for RNA sample preparation and Dr. Chanshuai Han for technical advice.

Funding: TMD and EAF received funding to support this project through the McGill Healthy Brains for Healthy Lives (HBHL) initiative, the CQDM FACs program, the Structural Genomics Consortium (SGC), The Sebastian and Ghislaine Van Berkom Foundation, the Alain and Sandra Bouchard Foundation, the Ellen Foundation and the Mowfaghian Foundation. EAF is supported by a Foundation grant from CIHR (FDN-154301), a Canada Research Chair (Tier 1) in Parkinson Disease and the Canadian Consortium on Neurodegeneration in Aging (CCNA). TMD is supported by a project grant from CIHR (PJT – 169095).

References

Akopian V, Andrews PW, Beil S, Benvenisty N, Brehm J, Christie M, Ford A, Fox V, Gokhale PJ, Healy L, Holm F, Hovatta O, Knowles BB, Ludwig TE, McKay RD, Miyazaki T, Nakatsuji N, Oh SK, Pera MF et al., 2010. Comparison of defined culture systems for feeder cell free propagation of human embryonic stem cells. In Vitro Cell Dev Biol Anim 46: 247-58. https://doi.org/10.1007/s11626-010-9297-z.

Allegrucci C, Yong LE., 2007. Differences between human embryonic stem cell lines. Hum Reprod Update 13:103-20. https://doi.org/10.1093/humupd/dml041.

Amps K, Andrews PW, Anyfantis G, Armstrong L, Avery S, Baharvand H, Baker J, Baker D, Munoz MB, Beil S, Benvenisty N, Ben-Yosef D, Biancotti JC, Bosman A, Brena RM, Brison D, Caisander G, Camarasa MV, Chen J et al., 2011. Screening ethnically diverse human embryonic stem cells identifies a chromosome 20 minimal amplicon conferring growth advantage. Nat Biotechnol 29: 1132-44. https://doi.org/10.1038/nbt.2051.

Assou S, Bouckenheimer J, De Vos J., 2018. Concise review: assessing the genome integrity of human induced pluripotent stem cells: what quality control metrics? Stem Cells 36: 814-821. https://doi.org/10.1002/stem.2797.

Attwood SW, Edel MJ., 2019. iPS-cell technology and the problem of genetic instability-Can it ever be safe for clinical use? J Clin Med 8: 288. https://doi.org/10.3390/jcm8030288.

Bai Q, Ramirez JM, Becker F, Pantesco V, Lavabre-Bertrand T, Hovatta O, Lemaitre JM, Pellestor F, De Vos J., 2015. Temporal analysis of genome alterations induced by single-cell passaging in human embryonic stem cells. Stem Cells Dev 24: 653-62. https://doi.org/10.1089/scd.2014.0292.

Baker D, Hirst AJ, Gokhale PJ, Juarez MA, Williams S, Wheeler M, Bean K, Allison TF, Moore HD, Andrews PW, Barbaric I., 2016. Detecting genetic mosaicism in cultures of human pluripotent stem cells. Stem Cell Reports 7: 998-1012. https://doi.org/10.1016/j.stemcr.2016.10.003.

Ben-David U, Mayshar Y, Benvenisty N., 2011. Large-scale analysis reveals acquisition of lineage-specific chromosomal aberrations in human adult stem cells. Cell Stem Cell 9: 97-102. https://doi.org/10.1016/j.stem.2011.06.013.

Brennand KJ, Simone A, Jou J, Gelboin-Burkhart C, Tran N, Sangar S, Li Y, Mu Y, Chen G, Yu D, McCarthy S, Sebat J, Gage FH., 2011. Modelling schizophrenia using human induced pluripotent stem cells. Nature 473: 221-5. https://doi.org/10.1038/nature09915.

Britanova O, de Juan Romero C, Cheung A, Kwan KY, Schwark M, Gyorgy A, Vogel T, Akopov S, Mitkovski M, Agoston D, Sestan N, Molnar Z, Tarabykin V., 2008. Satb2 is a postmitotic determinant for upper-layer neuron specification in the neocortex. Neuron 57: 378-92. https://doi.org/10.1016/j.neuron.2007.12.028.

Cabrera CM, Cobo F, Nieto A, Cortes JL, Montes RM, Catalina P, Concha A., 2006. Identity tests: determination of cell line cross-contamination. Cytotechnology 51: 45-50. https://doi.org/10.1007/s10616-006-9013-8.

Chatterjee R., 2007. Cell biology. Cases of mistaken identity. Science 315: 928-31. https://doi.org/10.1126/science.315.5814.928.

Chambers SM, Fasano CA, Papapetrou EP, Tomishima M, Sadelain M, Studer L., 2009. Highly efficient neural conversion of human ES and iPS cells by dual inhibition of SMAD signaling. Nat Biotechnol 27: 275-80. https://doi.org/10.1038/nbt.1529.

Chen G, Gulbranson DR, Hou Z, Bolin JM, Ruotti V, Probasco MD, Smuga-Otto K, Howden SE, Diol NR, Propson NE, Wagner R, Lee GO, Antosiewicz-Bourget J, Teng JM, Thomson JA., 2011. Chemically defined conditions for human iPSC derivation and culture. Nat Methods 8: 424-9. https://doi.org/10.1038/nmeth.1593.

Chin MH, Mason MJ, Xie W, Volinia S, Singer M, Peterson C, Ambartsumyan G, Aimiuwu O, Richter L, Zhang J, Khvorostov I, Ott V, Grunstein M, Lavon N, Benvenisty N, Croce CM, Clark AT, Baxter T, Pyle AD, Teitell MA et al., 2009. Induced pluripotent stem cells and embryonic stem cells are distinguished by gene expression signatures. Cell Stem Cell 5: 111-23. https://doi.org/10.1016/j.stem.2009.06.008.

D'Amour KA, Agulnick AD, Eliazer S, Kelly OG, Kroon E, Baetge EE., 2005. Efficient differentiation of human embryonic stem cells to definitive endoderm. Nat Biotechnol 23: 1534-41. https://doi.org/10.1038/nbt1163.

Daley GQ., 2012. The promise and perils of stem cell therapeutics. Cell Stem Cell 10: 740-749. https://doi.org/10.1016/j.stem.2012.05.010.

Daniszewski M, Nguyen Q, Chy HS, Singh V, Crombie DE, Kulkarni T, Liang HH, Sivakumaran P, Lidgerwood GE, Hernandez D, Conquest A, Rooney LA, Chevalier S, Andersen SB, Senabouth A, Vickers JC, Mackey DA, Craig JE, Laslett AL, Hewitt AW et al., 2018. Single-cell profiling identifies key pathways expressed by iPSCs cultured in different commercial media. iScience 7: 30-39. https://doi.org/10.1016/j.isci.2018.08.016.

Dolgin E., 2010. Putting stem cells to the test. Nat Med 16: 1354-7. https://doi.org/10.1038/nm1210-1354.

Draper JS, Smith K, Gokhale P, Moore HD, Maltby E, Johnson J, Meisner L, Zwaka TP, Thomson JA, Andrews PW., 2004. Recurrent gain of chromosomes 17q and 12 in cultured human embryonic stem cells. Nat Biotechnol 22: 53-4. https://doi.org/10.1038/nbt922.

Engle SJ, Blaha L, Kleiman RJ., 2018. Best practices for translational disease modeling using human iPSC-derived neurons. Neuron 100: 783-797. https://doi.org/10.1016/j.neuron.2018.10.033.

Feoktistova M, Geserick P, Leverkus M., 2016. Crystal violet assay for determining viability of cultured cells. Cold Spring Harb Protoc 2016: pdb prot087379. https://doi.org/10.1101/pdb.prot087379.

Ferland RJ, Cherry TJ, Preware PO, Morrisey EE, Walsh CA., 2003. Characterization of Foxp2 and Foxp1 mRNA and protein in the developing and mature brain. J Comp Neurol 460: 266-79. https://doi.org/10.1002/cne.10654.

Fu Y, Foden JA, Khayter C, Maeder ML, Reyon D, Joung JK, Sander JD., 2013. High-frequency off-target mutagenesis induced by CRISPR-Cas nucleases in human cells. Nat Biotechnol 31: 822-6. https://doi.org/10.1038/nbt.2623.

Hey CAB, Saltokova KB, Bisgaard HC, Moller LB., 2018. Comparison of two different culture conditions for derivation of early hiPSC. Cell Biol Int 42: 1467-1473. https://doi.org/10.1002/cbin.10966.

Hussein SM, Batada NN, Vuoristo S, Ching RW, Autio R, Narva E, Ng S, Sourour M, Hamalainen R, Olsson C, Lundin K, Mikkola M, Trokovic R, Peitz M, Brustle O, Bazett-Jones DP, Alitalo K, Lahesmaa R, Nagy A, Otonkoski T., 2011. Copy number variation and selection during reprogramming to pluripotency. Nature 471: 58-62. https://doi.org/10.1038/nature09871.

Inzunza J, Sahlen S, Holmberg K, Stromberg AM, Teerijoki H, Blennow E, Hovatta O, Malmgren H., 2004. Comparative genomic hybridization and karyotyping of human embryonic stem cells reveals the occurrence of an isodicentric X chromosome after long-term cultivation. Mol Hum Reprod 10: 461-6. https://doi.org/10.1093/molehr/gah051.

Israel MA, Yuan SH, Bardy C, Reyna SM, Mu Y, Herrera C, Hefferan MP, Van Gorp S, Nazor KL, Boscolo FS, Carson CT, Laurent LC, Marsala M, Gage FH, Remes AM, Koo EH, Goldstein LS., 2012. Probing sporadic and familial Alzheimer's disease using induced pluripotent stem cells. Nature 482: 216-20. https://doi.org/10.1038/nature10821.

Itskovitz-Eldor J, Schuldiner M, Karsenti D, Eden A, Yanuka O, Amit M, Soreq H, Benvenisty N., 2000. Differentiation of human embryonic stem cells into embryoid bodies compromising the three embryonic germ layers. Mol Med 6: 88-95. https://doi.org/10.1007/BF03401776.

Koehler KR, Tropel P, Theile JW, Kondo T, Cummins TR, Viville S, Hashino E., 2011. Extended passaging increases the efficiency of neural differentiation from induced pluripotent stem cells. BMC Neurosci 12: 82. https://doi.org/10.1186/1471-2202-12-82.

Lamm N, Ben-David U, Golan-Lev T, Storchova Z, Benvenisty N, Kerem B., 2016. Genomic instability in human pluripotent stem cells arises from replicative stress and chromosome condensation defects. Cell Stem Cell 18: 253-61. https://doi.org/10.1016/j.stem.2015.11.003.

Laurent LC, Ulitsky I, Slavin I, Tran H, Schork A, Morey R, Lynch C, Harness JV, Lee S, Barrero MJ, Ku S, Martynova M, Semechkin R, Galat V, Gottesfeld J, Izpisua Belmonte JC, Murry C, Keirstead HS, Park HS, Schmidt U et al., 2011. Dynamic changes in the copy number of pluripotency and cell proliferation genes in human ESCs and iPSCs during reprogramming and time in culture. Cell Stem Cell 8: 106-18. https://doi.org/10.1016/j.stem.2010.12.003.

Lefort N, Feyeux M, Bas C, Feraud O, Bennaceur-Griscelli A, Tachdjian G, Peschanski M, Perrier AL., 2008. Human embryonic stem cells reveal recurrent genomic instability at 20q11.21. Nat Biotechnol 26: 1364-6. https://doi.org/10.1038/nbt.1509.

Lowry WE, Richter L, Yachechko R, Pyle AD, Tchieu J, Sridharan R, Clark AT, Plath K., 2008. Generation of human induced pluripotent stem cells from dermal fibroblasts. Proc Natl Acad Sci U S A 105: 2883-8. https://doi.org/10.1073/pnas.0711983105.

Ludwig TE, Levenstein ME, Jones JM, Berggren WT, Mitchen ER, Frane JL, Crandall LJ, Daigh CA, Conard KR, Piekarczyk MS, Llanas RA, Thomson JA., 2006. Derivation of human embryonic stem cells in defined conditions. Nat Biotechnol 24: 185-7. https://doi.org/10.1038/nbt1177.

Lund RJ, Narva E, Lahesmaa R., 2012. Genetic and epigenetic stability of human pluripotent stem cells. Nat Rev Genet 13: 732-44. https://doi.org/10.1038/nrg3271.

Maherali N, Sridharan R, Xie W, Utikal J, Eminli S, Arnold K, Stadtfeld M, Yachechko R, Tchieu J, Jaenisch R, Plath K, Hochedlinger K,. 2007. Directly reprogrammed fibroblasts show global epigenetic remodeling and widespread tissue contribution. Cell Stem Cell 1: 55-70. https://doi.org/10.1016/j.stem.2007.05.014.

Mandai M, Watanabe A, Kurimoto Y, Hirami Y, Morinaga C, Daimon T, Fujihara M, Akimaru H, Sakai N, Shibata Y, Terada M, Nomiya Y, Tanishima S, Nakamura M, Kamao H, Sugita S, Onishi A, Ito T, Fujita K, Kawamata S et al., 2017. Autologous induced stem-cell-derived retinal cells for macular degeneration. N Engl J Med 376: 1038-1046. https://www.nejm.org/doi/10.1056/NEJMoa1608368.

Martin U., 2017. Genome stability of programmed stem cell products. Adv Drug Deliv Rev 120: 108-117. https://doi.org/10.1016/j.addr.2017.09.004.

Matoba R, Niwa H, Masui S, Ohtsuka S, Carter MG, Sharov AA, Ko MS., 2006. Dissecting Oct3/4-regulated gene networks in embryonic stem cells by expression profiling. PLoS One 1: e26. https://doi.org/10.1371/journal.pone.0000026.

Mikkelsen TS, Hanna J, Zhang X, Ku M, Wernig M, Schorderet P, Bernstein BE, Jaenisch R, Lander ES, Meissner A., 2008. Dissecting direct reprogramming through integrative genomic analysis. Nature 454: 49-55. https://doi.org/10.1038/nature07056.

Muller FJ, Brandl B, Loring JF., 2008. Assessment of human pluripotent stem cells with PluriTest. In StemBook, Cambridge (MA): doi: 10.3824/stembook.1.84.1.

Narva E, Autio R, Rahkonen N, Kong L, Harrison N, Kitsberg D, Borghese L, Itskovitz-Eldor J, Rasool O, Dvorak P, Hovatta O, Otonkoski T, Tuuri T, Cui W, Brustle O, Baker D, Maltby E, Moore HD, Benvenisty N, Andrews PW et al., 2010. High-resolution DNA analysis of human embryonic stem cell lines reveals culture-induced copy number changes and loss of heterozygosity. Nat Biotechnol 28: 371-7. https://doi.org/10.1038/nbt.1615.

Nguyen QH, Lukowski SW, Chiu HS, Senabouth A, Bruxner TJC, Christ AN, Palpant NJ, Powell JE., 2018. Single-cell RNA-seq of human induced pluripotent stem cells reveals cellular heterogeneity and cell state transitions between subpopulations. Genome Res 28: 1053-1066. http://www.genome.org/cgi/doi/10.1101/gr.223925.117.

O'Malley J, Skylaki S, Iwabuchi KA, Chantzoura E, Ruetz T, Johnsson A, Tomlinson SR, Linnarsson S, Kaji K., 2013. High-resolution analysis with novel cell-surface markers identifies routes to iPS cells. Nature 499: 88-91. https://doi.org/10.1038/nature12243.

Okita K, Ichisaka T, Yamanaka S., 2007. Generation of germline-competent induced pluripotent stem cells. Nature 448: 313-7. https://doi.org/10.1038/nature05934.

Papapetrou EP, Tomishima MJ, Chambers SM, Mica Y, Reed E, Menon J, Tabar V, Mo Q, Studer L, Sadelain M., 2009. Stoichiometric and temporal requirements of Oct4, Sox2, Klf4, and c-Myc expression for efficient human iPSC induction and differentiation. Proc Natl Acad Sci U S A 106: 12759-64. https://doi.org/10.1073/pnas.0904825106.

Peterson SE, Westra JW, Rehen SK, Young H, Bushman DM, Paczkowski CM, Yung YC, Lynch CL, Tran HT, Nickey KS, Wang YC, Laurent LC, Loring JF, Carpenter MK, Chun J., 2011. Normal human pluripotent stem cell lines exhibit pervasive mosaic aneuploidy. PLoS One 6: e23018. https://doi.org/10.1371/journal.pone.0023018.

Rohani L, Johnson AA, Naghsh P, Rancourt DE, Ulrich H, Holland H., 2018. Concise review: molecular cytogenetics and quality control: clinical guardians for pluripotent stem cells. Stem Cells Transl Med 7: 867-875. https://doi.org/10.1002/sctm.18-0087.

Ruiz S, Lopez-Contreras AJ, Gabut M, Marion RM, Gutierrez-Martinez P, Bua S, Ramirez O, Olalde I, Rodrigo-Perez S, Li H, Marques-Bonet T, Serrano M, Blasco MA, Batada NN,

Fernandez-Capetillo O., 2015. Limiting replication stress during somatic cell reprogramming reduces genomic instability in induced pluripotent stem cells. Nat Commun 6: 8036. https://doi.org/10.1038/ncomms9036.

Sareen D, McMillan E, Ebert AD, Shelley BC, Johnson JA, Meisner LF, Svendsen CN., 2009. Chromosome 7 and 19 trisomy in cultured human neural progenitor cells. PLoS One 4: e7630. https://doi.org/10.1371/journal.pone.0007630.

Scotto L, Narayan G, Nandula SV, Arias-Pulido H, Subramaniyam S, Schneider A, Kaufmann AM, Wright JD, Pothuri B, Mansukhani M, Murty VV., 2008. Identification of copy number gain and overexpressed genes on chromosome arm 20q by an integrative genomic approach in cervical cancer: potential role in progression. Genes Chromosomes Cancer 47: 755-65. https://doi.org/10.1002/gcc.20577.

Son MY, Choi H, Han YM, Cho YS., 2013. Unveiling the critical role of REX1 in the regulation of human stem cell pluripotency. Stem Cells 31: 2374-87. https://doi.org/10.1002/stem.1509.

Sugitani Y, Nakai S, Minowa O, Nishi M, Jishage K, Kawano H, Mori K, Ogawa M, Noda T., 2002. Brn-1 and Brn-2 share crucial roles in the production and positioning of mouse neocortical neurons. Genes Dev 16: 1760-5. doi:10.1101/gad.978002.

Sullivan S, Stacey GN, Akazawa C, Aoyama N, Baptista R, Bedford P, Bennaceur Griscelli A, Chandra A, Elwood N, Girard M, Kawamata S, Hanatani T, Latsis T, Lin S, Ludwig TE, Malygina T, Mack A, Mountford JC, Noggle S, Pereira LV et al., 2018. Quality control guidelines for clinical-grade human induced pluripotent stem cell lines. Regen Med 13: 859-866. https://doi.org/10.2217/rme-2018-0095.

Taapken SM, Nisler BS, Newton MA, Sampsell-Barron TL, Leonhard KA, McIntire EM, Montgomery KD., 2011. Karotypic abnormalities in human induced pluripotent stem cells and embryonic stem cells. Nat Biotechnol 29: 313-4. https://doi.org/10.1038/nbt.1835.

Takahashi K, Tanabe K, Ohnuki M, Narita M, Ichisaka T, Tomoda K, Yamanaka S., 2007. Induction of pluripotent stem cells from adult human fibroblasts by defined factors. Cell 131: 861-72. https://doi.org/10.1016/j.cell.2007.11.019.

Takahashi K, Yamanaka S., 2006. Induction of pluripotent stem cells from mouse embryonic and adult fibroblast cultures by defined factors. Cell 126: 663-76. https://doi.org/10.1016/j.cell.2006.07.024.

Tano K, Yasuda S, Kuroda T, Saito H, Umezawa A, Sato Y., 2014. A novel in vitro method for detecting undifferentiated human pluripotent stem cells as impurities in cell therapy products using a highly efficient culture system. PLoS One 9: e110496. https://doi.org/10.1371/journal.pone.0110496.

Ungrin MD, Joshi C, Nica A, Bauwens C, Zandstra PW., 2008. Reproducible, ultra high-throughput formation of multicellular organization from single cell suspension-derived human embryonic stem cell aggregates. PLoS One 3: e1565. https://doi.org/10.1371/journal.pone.0001565.

Wen W, Zhang JP, Xu J, Su RJ, Neises A, Ji GZ, Yuan W, Cheng T, Zhang XB., 2016. Enhanced generation of integration-free iPSCs from human adult peripheral blood mononuclear cells with an optimal combination of episomal vectors. Stem Cell Reports 6: 873-884. https://doi.org/10.1016/j.stemcr.2016.04.005.

Wernig M, Meissner A, Foreman R, Brambrink T, Ku M, Hochedlinger K, Bernstein BE, Jaenisch R., 2007. In vitro reprogramming of fibroblasts into a pluripotent ES-cell-like state. Nature 448: 318-24. https://doi.org/10.1038/nature05944.

Xu RH, Chen X, Li DS, Li R, Addicks GC, Glennon C, Zwaka TP, Thomson JA., 2002. BMP4 initiates human embryonic stem cell differentiation to trophoblast. Nat Biotechnol 20: 1261-4. https://doi.org/10.1038/nbt761.

Xu RH, Sampsell-Barron TL, Gu F, Root S, Peck RM, Pan G, Yu J, Antosiewicz-Bourget J, Tian S, Stewart R, Thomson JA., 2008. NANOG is a direct target of TGFbeta/activin-mediated SMAD signaling in human ESCs. Cell Stem Cell 3: 196-206. https://doi.org/10.1016/j.stem.2008.07.001.

Yaffe MP, Noggle SA, Solomon SL., 2016. Raising the standards of stem cell line quality. Nat Cell Biol 18: 236-7. https://doi.org/10.1038/ncb3313.

Yamaguchi S, Hirano K, Nagata S, Tada T., 2011. Sox2 expression effects on direct reprogramming efficiency as determined by alternative somatic cell fate. Stem Cell Res 6: 177-86. https://doi.org/10.1016/j.scr.2010.09.004.

Yang L, Grishin D, Wang G, Aach J, Zhang CZ, Chari R, Homsy J, Cai X, Zhao Y, Fan JB, Seidman C, Seidman J, Pu W, Church G., 2014. Targeted and genome-wide sequencing reveal single nucleotide variations impacting specificity of Cas9 in human stem cells. Nat Commun 5: 5507. https://doi.org/10.1038/ncomms6507.

Zhang SC, Wernig M, Duncan ID, Brustle O, Thomson JA., 2001. In vitro differentiation of transplantable neural precursors from human embryonic stem cells. Nat Biotechnol 19: 1129-33. https://doi.org/10.1038/nbt1201-1129.

Table 1. Overview of hiPSC profiles

Cell line	Donor	Cell Type	Donor age	Sex[1]	Cell source	Reprogramming	Media[2]
H9		ESC	NA	F	WiCell		mTeSR1
NCRM1	A	cord blood	NA	M	NIH	Episomal	mTeSR1
KYOU-DXR0109B	B	fibroblast	36	F	ATCC	Sendai virus	mTeSR1
AIW002-02	C	PBMC	37	M	The Neuro	Sendai virus	mTeSR1
AJC001-5	C	fibroblast	37	M	The Neuro	Sendai virus	mTeSR1
AJG001-C4	C	PBMC	37	M	The Neuro	Episomal	mTeSR1
TD02	D	PBMC	48	F	The Neuro	Episomal	mTeSR1
3448	E	PBMC	48	M	The Neuro	Episomal	E8
3450	F	PBMC	37	M	The Neuro	Episomal	E8
AJD002-3	G	PBMC	44	M	The Neuro	Sendai virus	E8
TD03	G	PBMC	44	M	The Neuro	Episomal	E8
TD10	H	PBMC	64	F	The Neuro	Episomal	E8
TD22	I	PBMC	59	M	The Neuro	Episomal	E8

[1] M, male; F, female; [2] optimal media for cell growth

The passage number of NEURO hiPSC lines are 8-12; H9: P30+P5; NCRM1: P50+P11; KYOU-DXR0109B: +P3 after cell had been purchased from ATCC, no passage information on product datasheet.

Table 2. Representative STR profiling of AJD002-3 and TD03 for authentication

	3059 PBMC		AJD002-3 iPSC		TD03 iPSC	
Marker	**Allele 1**	**Allele 2**	**Allele 1**	**Allele 2**	**Allele 1**	**Allele 2**
AMEL	X	Y	X	Y	X	Y
CSF1PO	11	12	11	12	11	12
D13S317	9	11	9	11	9	11
D16S539	9	11	9	11	9	11
D21S11	28	30	28	30	28	30
D5S818	9	11	9	11	9	11
D7S820	12	12	12	12	12	12
TH01	6	9	6	9	6	9
TPOX	8	9	8	9	8	9
vWA	14	15	14	15	14	15

Figure Legends

Fig. 1. Standardized workflow for analyzing the quality and differentiation potential of hiPSCs.

Schematic representation of a multistep QC workflow to monitor the morphology and proliferation of newly generated iPSCs in two different media (mTeSR1 and E8). The comprehensive phenotyping of each iPSC line through STR profiling, genome stability, pluripotency and their ability to form the three germ layers, with a focus on cortical neurons of the ectodermal lineage have been evaluated thoroughly before using it in downstream applications.

Figure 2. HiPSC growth and proliferation under different conditions. (**A**) Representative daily morphology of hiPSCs maintained in mTeSR1 or E8 media. Both cell lines show smooth-edged, tightly packed cells with a large nucleus-to-cytoplasm ratio. AJG001-C4 cells grows slightly better in mTeSR1 media, while 3448 proliferate better in E8. (**B**) CV assay of representative cell lines grown in mTeSR1 and E8. AJC001-5 grows well in both media. AJG001-C4 grows better in mTeSR1 media, while AJD002-3 cells proliferate best in E8. (**C**) Quantification of the hiPSC's survival and growth in different media. The CV stain was dissolved in methanol and optical density measured at 540 nm (OD540). The mean and the standard deviation are from 6 replicates from two independent experiments.

Figure 3. Expression of pluripotency markers in hiPSCs. (**A**) Phase contrast images and ICC for pluripotency markers SSEA-4, OCT3/4, NANOG and Tra-1-60 with HO342 nucleic acid counterstain. (**B**) Quantification of OCT3/4 positive cells or SSEA-4-positive cells in (**A**). (**C**) q-PCR for mRNA expression of pluripotency genes POU5F1, NANOG, c-MYC, KLF4, SOX2 and ZFP42 in hiPSCs compared to H9 ESC. mRNA expression in H9 was set as 1.0. The mean and SD are from technical triplicates from two independent experiments.

Figure 4. Genomic stability analysis of hiPSCs. (**A**) Karyotyping and G-band analyses showing examples of one normal (left) and one abnormal hiPSC karyotype (right). An apparently balanced translocation between the long (q) arm of chromosome X and the short (p) arm of chromosome 2 is present in TD10 (red arrow). (**B**) q-PCR based genetic analysis to detect small chromosome abnormalities in all hiPSC lines. The copy numbers of chr1q, chr8q, chr10p, chr12p, chr17q, chr18q, chr20q and chrXp were normalized to chr4p expression set to be 2. Error bars show standard deviation from technical triplicates from two independent experiments. There are no abnormalities within critical regions in The Neuro cell

lines, while NCRM1 and KYOU-DXR0109 have amplification of chr20q (blue arrow). TD03 shows a slight increase in chr20q, however this is not above the threshold of expected variation.

Figure 5. Differentiation of hiPSCs into three germ layers. (**A**) Representative phase contrast images of EB formation (left) and differentiation into three germ layers by ICC with the ectoderm marker PAX6, the mesoderm marker SMA and the endoderm marker VIM (indicated above images). Nuclei are counterstained with HO 342. (**B**) q-PCR for mRNA expression of three germ layer genes. Quantification of expression of the ectoderm markers PAX6, NCAM1, mesoderm marker MIXL1 and endoderm marker VIM in hiPSCs compared to H9 ESC. mRNA expression in H9 was set as 1.0. The mean and SD are from technical triplicates from two independent experiments.

Figure 6. Differentiation of hiPSC into forebrain cortical neurons. (**A**) Schematic representation of the *in vitro* differentiation protocol used to generate cortical neurons from hiPSC. Boxes indicate differentiation state. This protocol was performed in 11 independent lines, with all lines performing similarly. (**B**) q-PCR for mRNA expression of neuronal markers MAP2, NCAM1 and TUBB3 in NPC and 4 weeks differentiated cortical neurons compared to IPSCs. mRNA expression in IPSC was set as 1.0. The mean and SD are from technical triplicates from two independent experiments. (**C**) Expression of cortical layer markers FOXP1 and SATB2 by q-PCR analysis of 4 weeks differentiated cortical neurons compared to iPSCs. mRNA expression in iPSC was set as 1.0. The mean and SD are from technical triplicates from two independent experiments.

Figure 7. Immunocytochemistry staining of hiPSC-derived cortical neurons. (**A**) Representative images of ICC stained cortical neurons from AJG001-C4, NCRM1, AJD002-3 and TD03 after 4 weeks neuronal differentiation. Cells were stained with MAP2 and Tuj1 neuronal markers, and cortical neuron markers Brn2 and Tbr1. Nuclei were counterstained with HO342. (**B**) Quantification of MAP2, Tuj1, Brn2 or Tbr1 positive cells in (**A**).

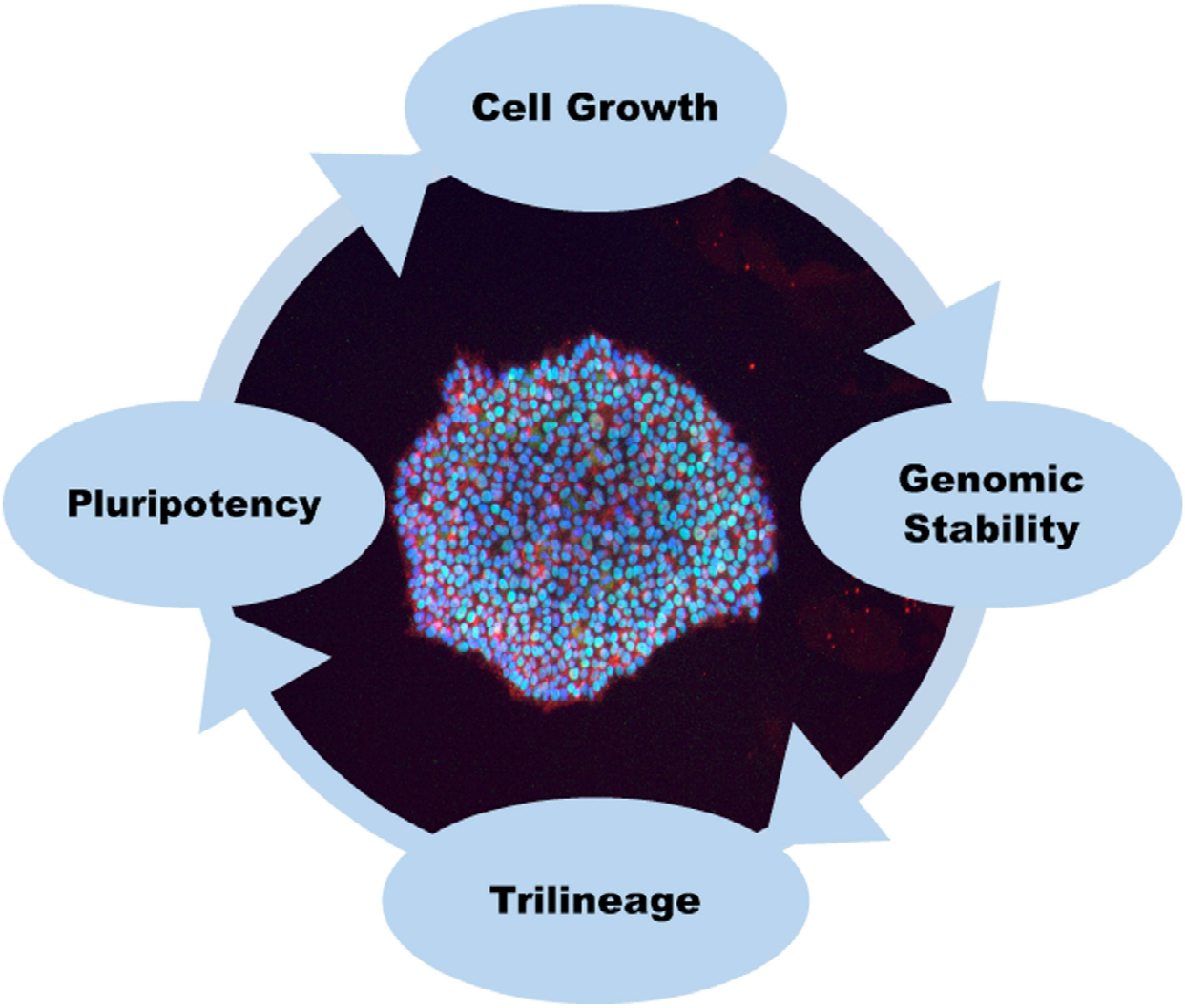

Chen et al, Figure 1

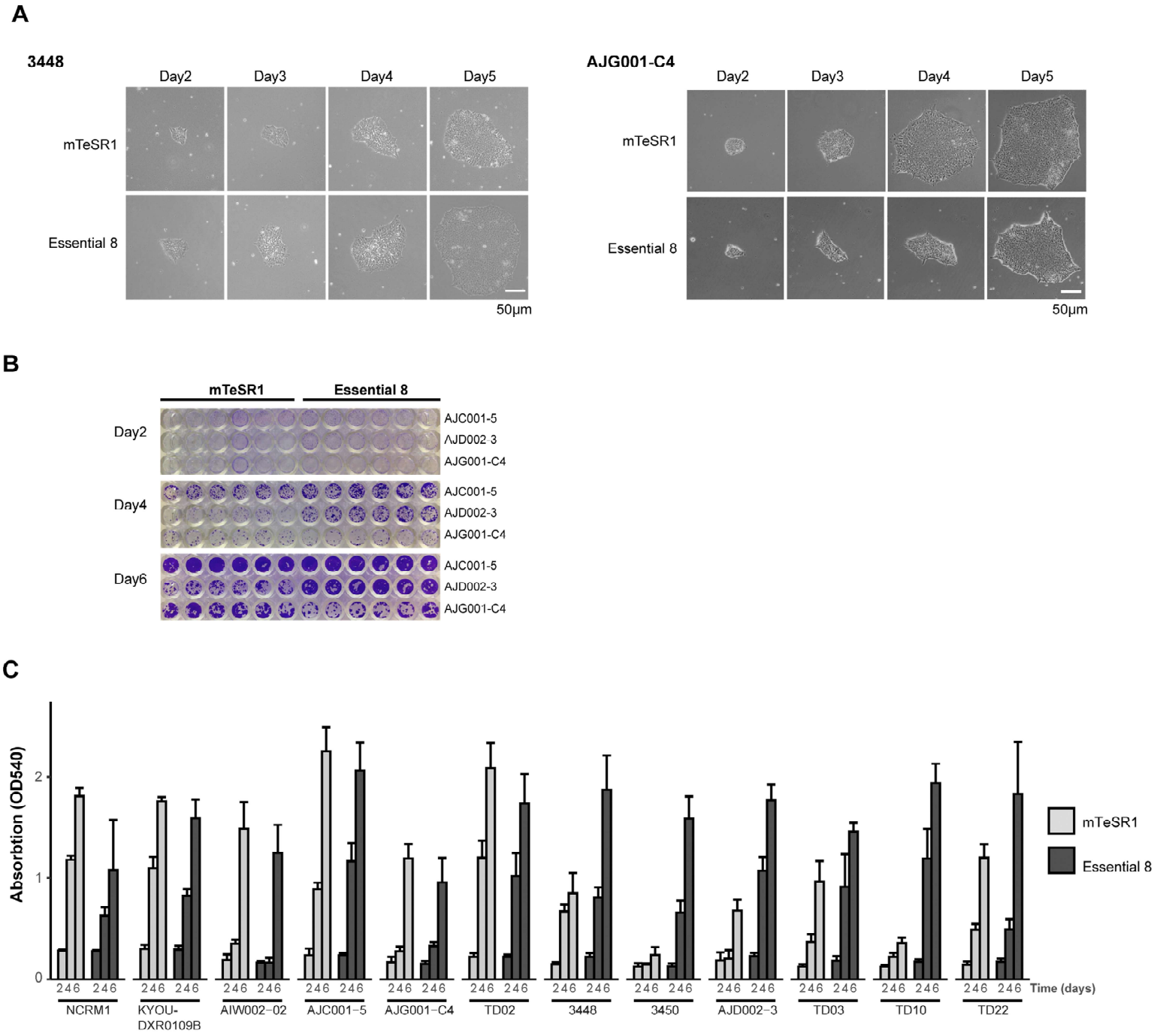

Chen et al, Figure 2

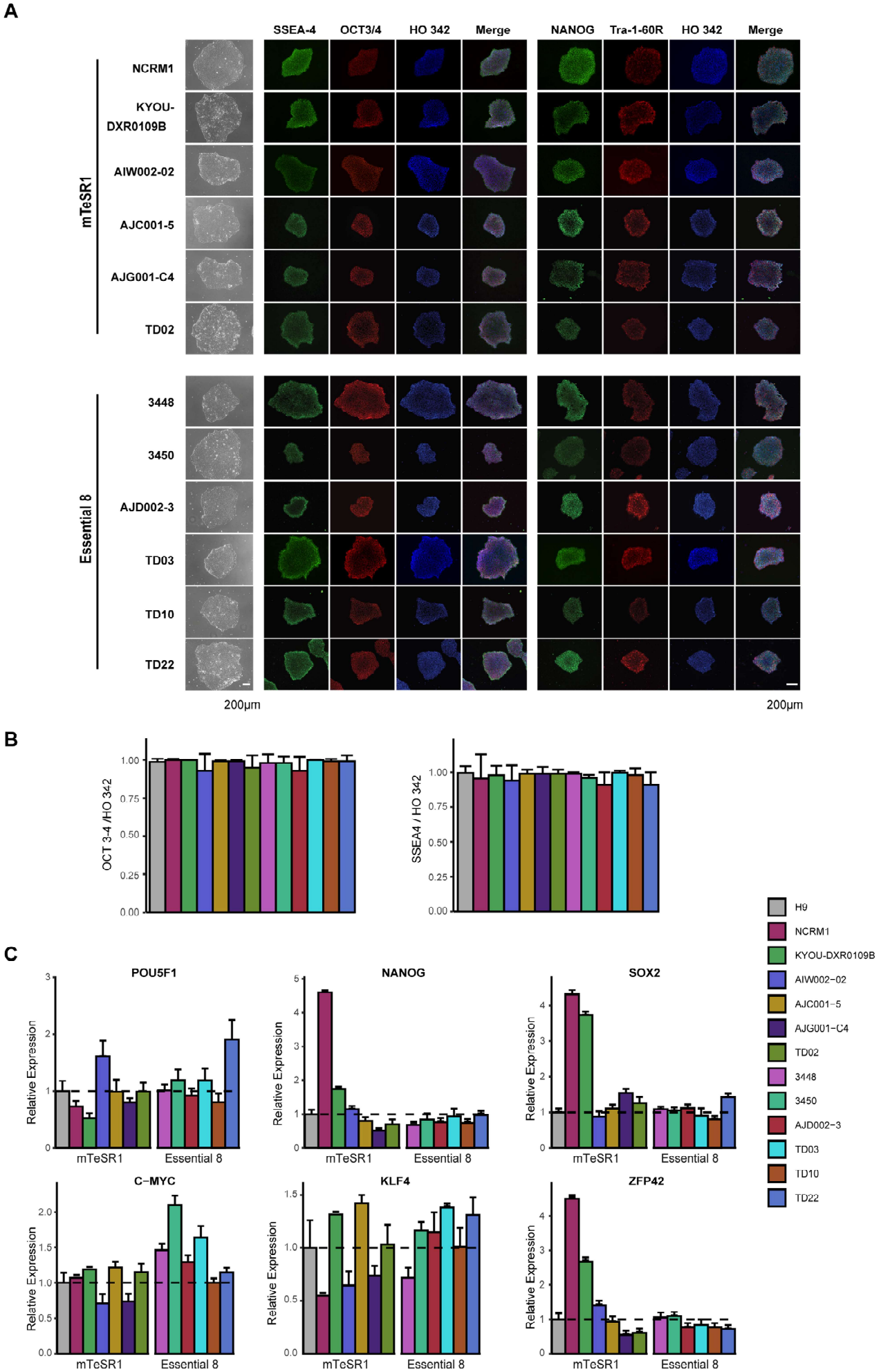

Chen et al, Figure 3

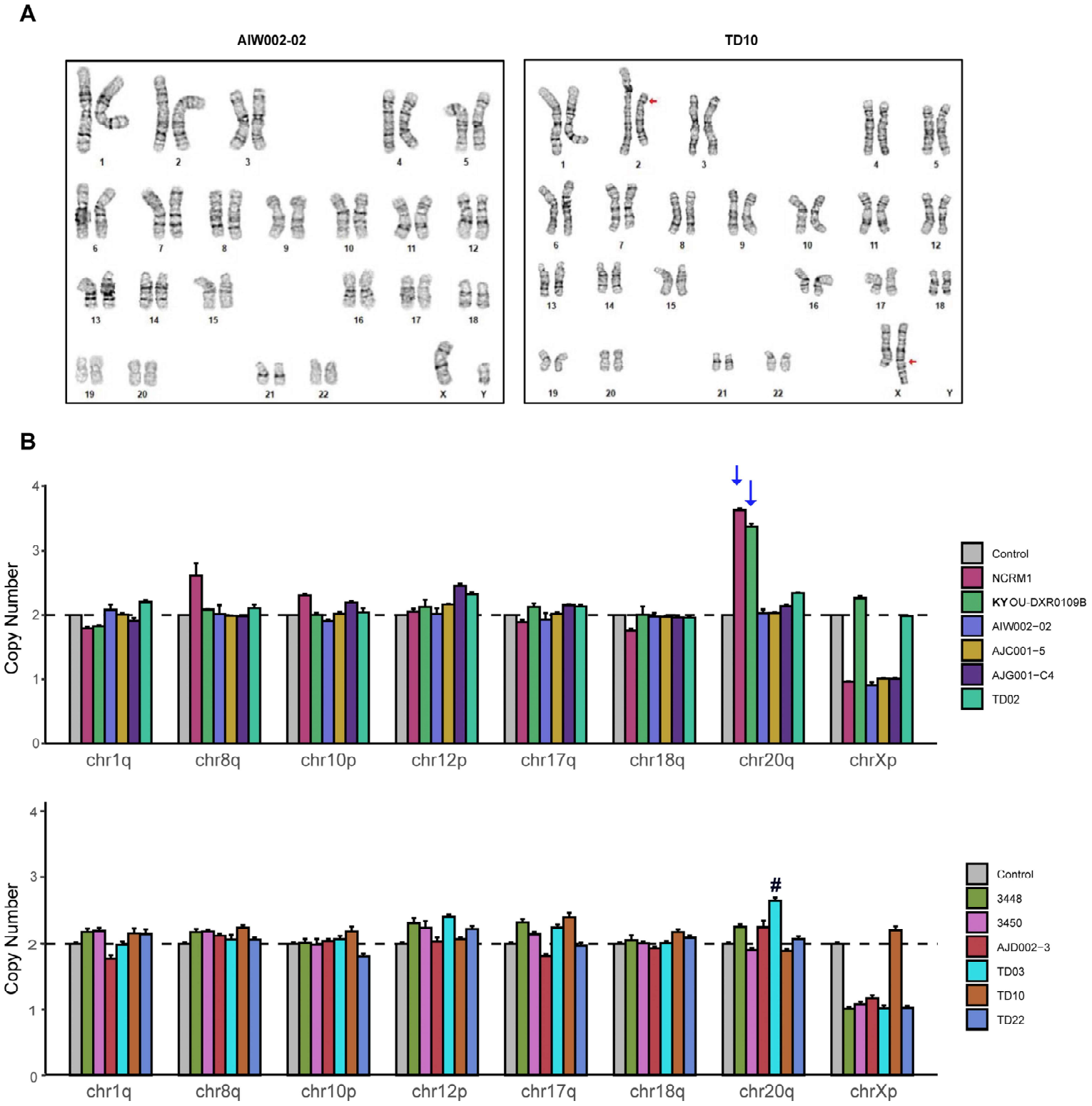

Chen et al, Figure 4

A

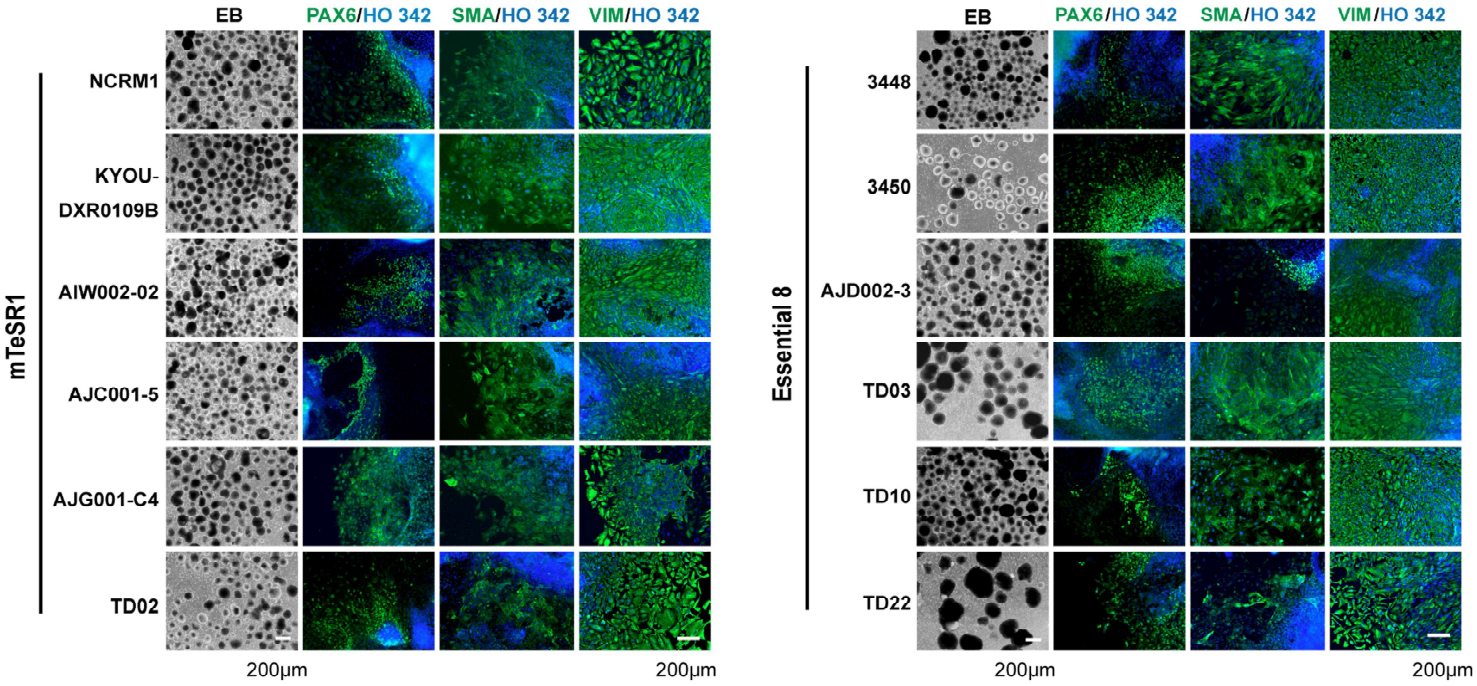

B

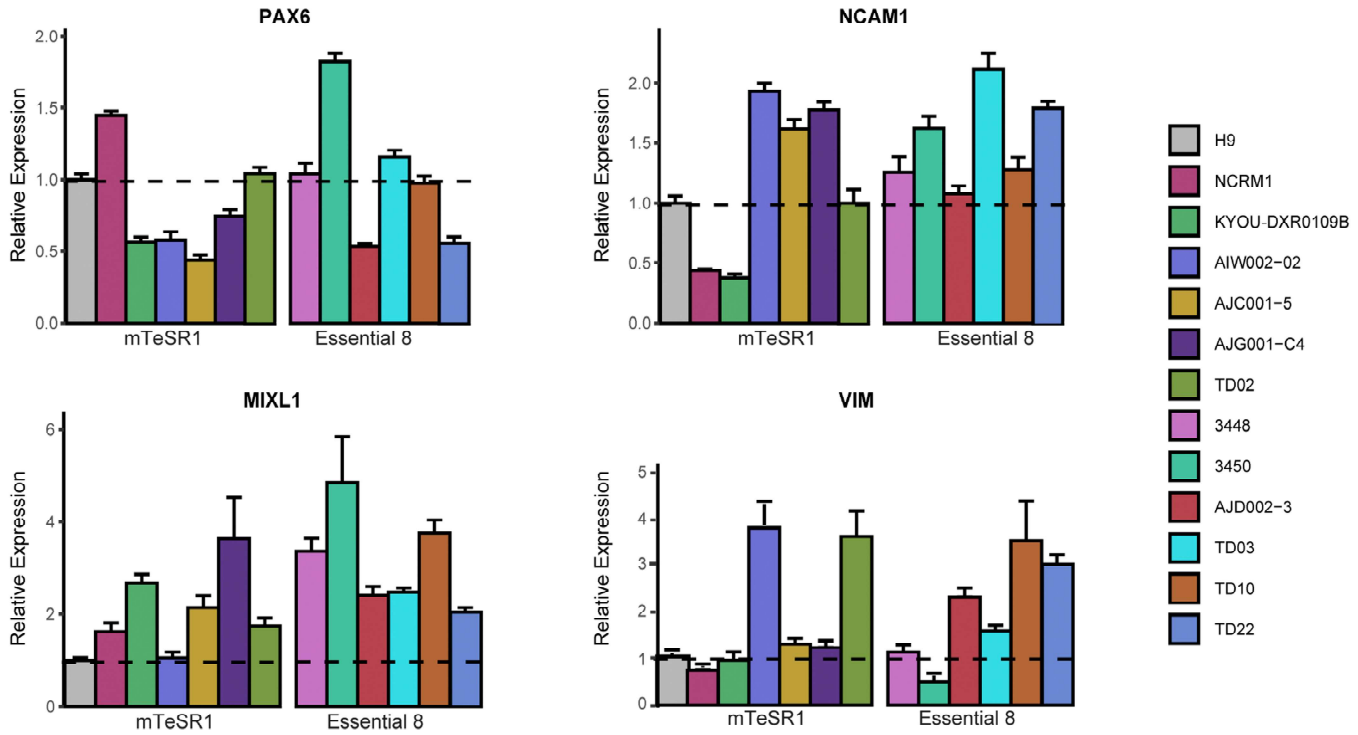

Chen et al, Figure 5

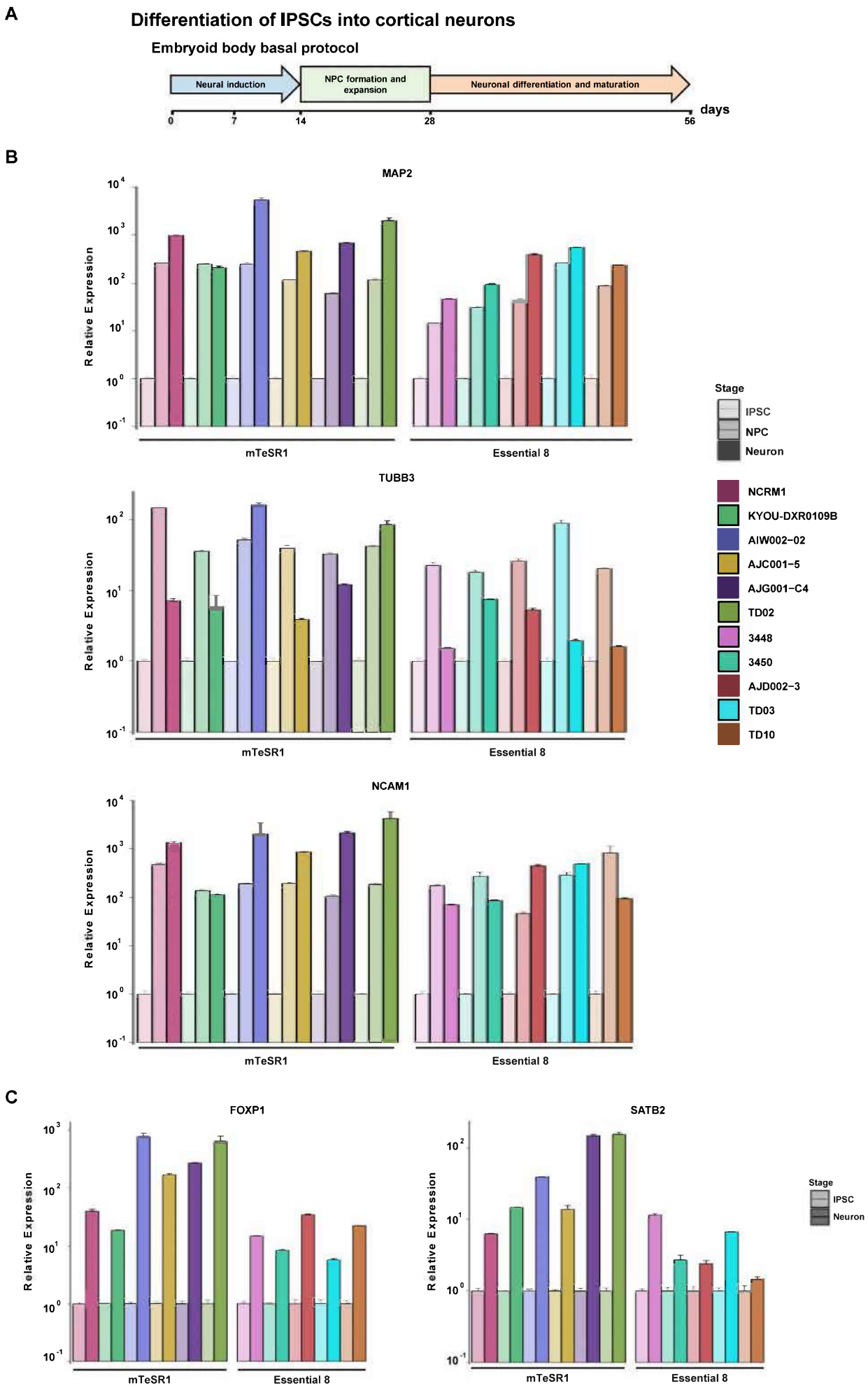

Chen et al, Figure 6

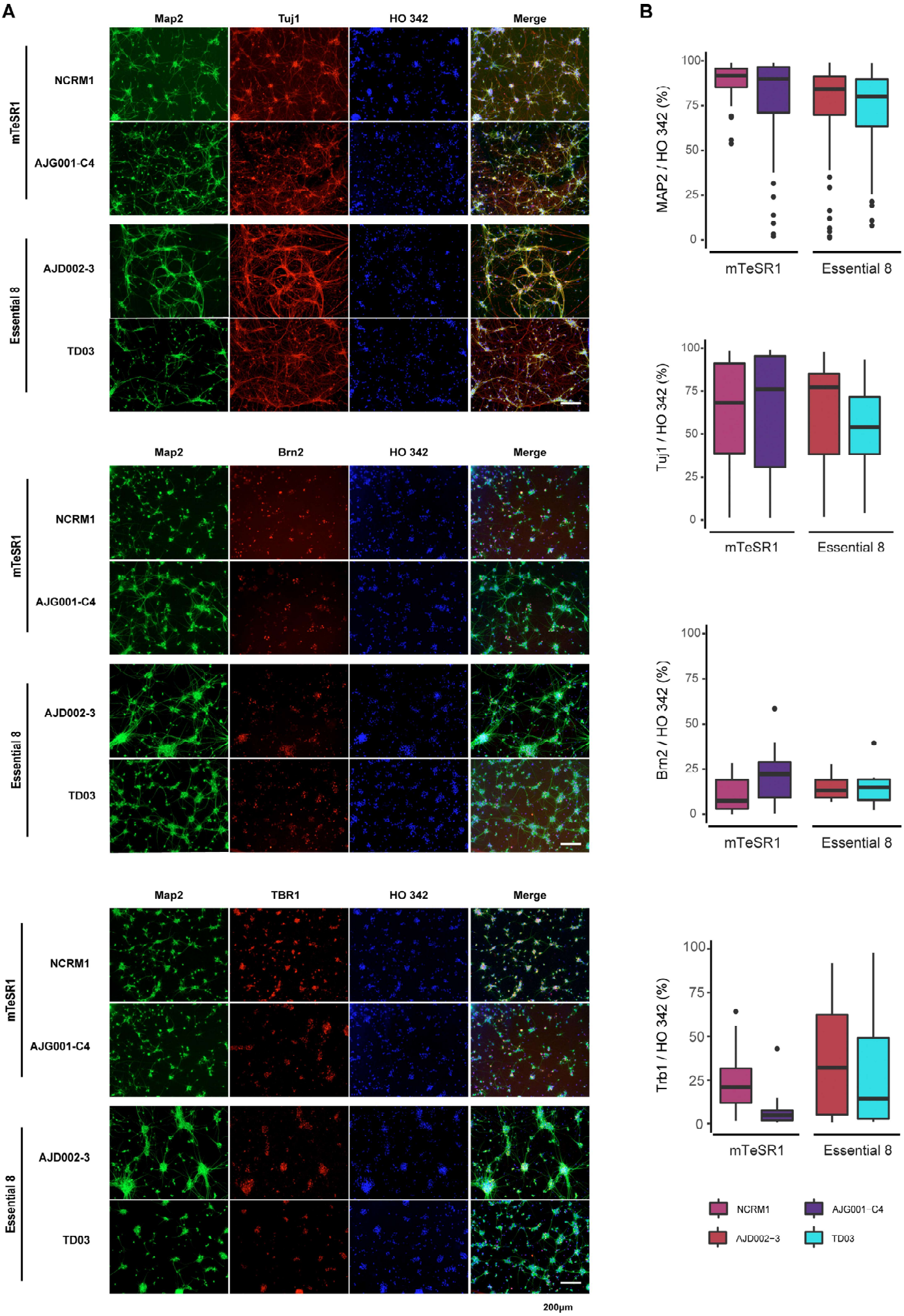

Chen et al, Figure 7

Supplementary Figure Legends

Fig. S1. HiPSC growth and proliferation profile in mTeSR1 or Essential 8 media. Related to Fig. 1. Crystal violet staining of hiPSCs grown in mTeSR1 and Essential 8 after day 2, 4 and 6 in culture.

Fig. S2. HiPSCs maintain a normal karyotype. Related to Fig. 3. Karyotyping and G-band analyses show 8 control hiPSC lines have normal 46, XY or 46, XX karyotypes.

Fig. S3. Characterization of hiPSC-derived NPCs. (**A**) Representative images of immunostained NPCs from AJG001-C4, NCRM1, AJD002-3 and TD03 hiPSC. Cells are stained with neural progenitor markers Nestin and SOX1, proliferative marker Ki67 and neuronal marker MAP2. Nuclei were counterstained with Hoechst 33342 at day 25. (**B**) Quantification of Nestin, MAP2, SOX1 or Ki67 positive cells in (**B**).

Fig. S4. Gene expression profiles in neural progenitor cells. (**A**) q-PCR for the mRNA expression of pluripotency markers POU5F1 and NANOG in NPC at day 25 of differentiation. The mRNA expression in iPSCs was set as 1.0. The mean and SD are from technical triplicates from two independent experiments. (**B**) q-PCR for the mRNA expression of mesoderm marker MIXL1 and endoderm marker AFP in NPC at day 25 of differentiation. mRNA expression in mesoderm or endoderm was set as 1.0. The mean and SD are from technical triplicates from two independent experiments. (**B**) Quantification of expression of neural progenitor maker Nestin, and the forebrain cortical NPC markers SLC1A3, PAX6 and ASCL1 as measured by q-PCR in NPC are compared to iPSCs. mRNA expression in iPSCs was set as 1.0. The mean and SD are from technical triplicates from two independent experiments.

Fig. S5. Comparison of gene expression levels in the neurons derived from iPSCs lines maintained in mTeSR1 to neurons from iPSCs maintained in E8. (**A**) The mRNA expression levels of neuronal markers MAP2, NCAM1 and TUBB3 are significantly higher in the neurons derived from iPSCs lines maintained in mTeSR1 (*: $p<0.05$). (**B**) The mRNA expression levels of cortical layers markers FOXG1 and SATB2 are significantly higher in the neurons derived from iPSCs lines maintained in mTeSR1 than that in Essential 8 (**: $p<0.01$).

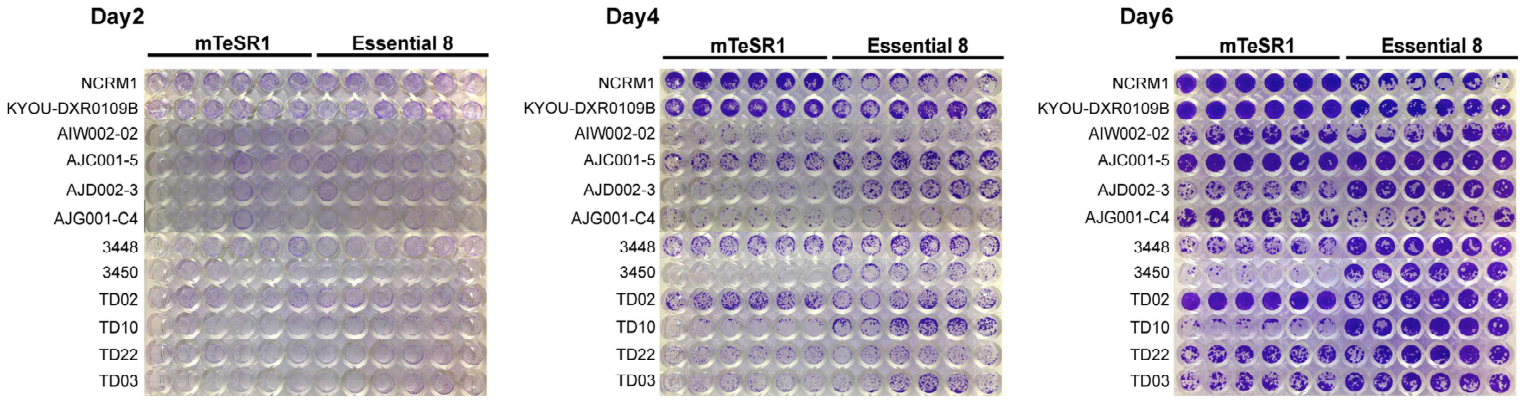

Chen et al, Supplementary Figure S1

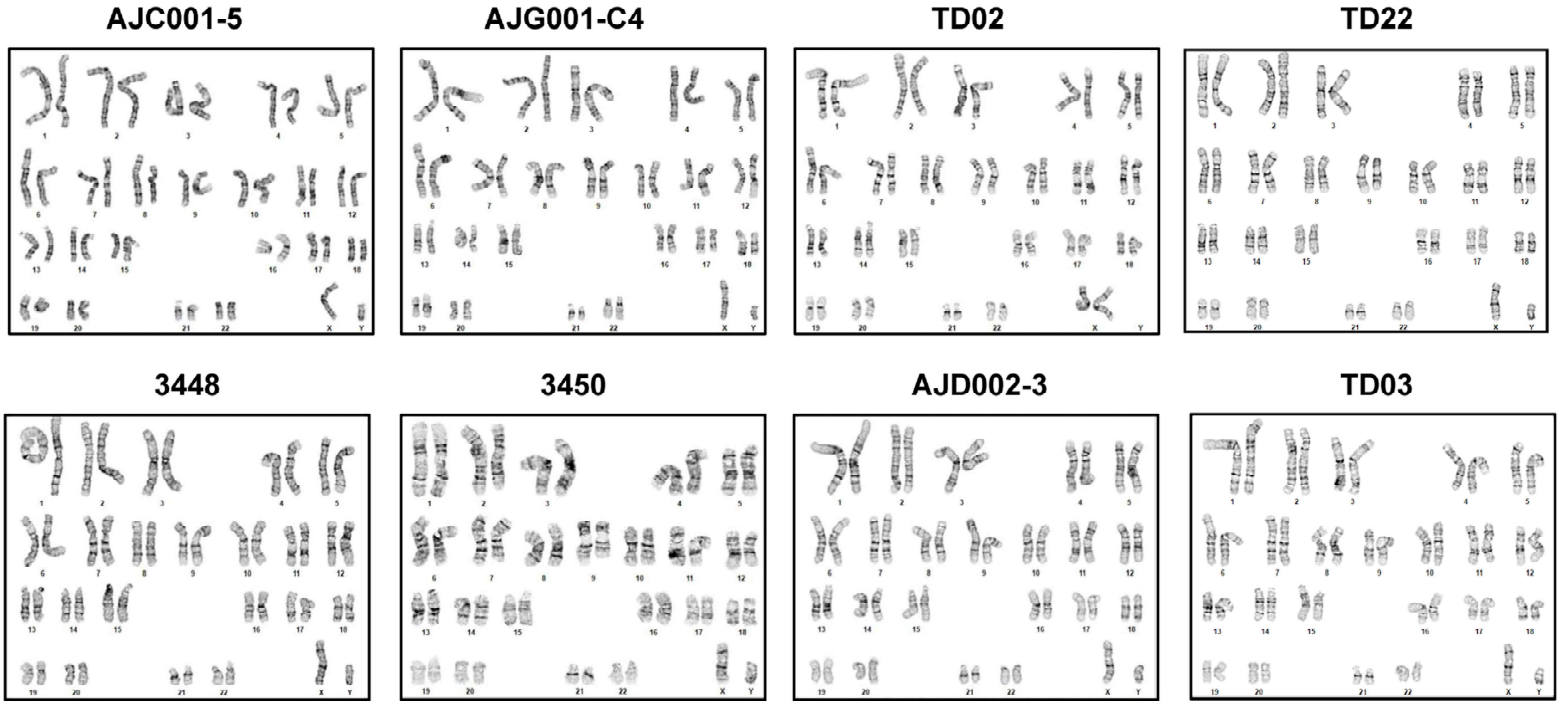

Chen et al, Supplementary Figure S2

A

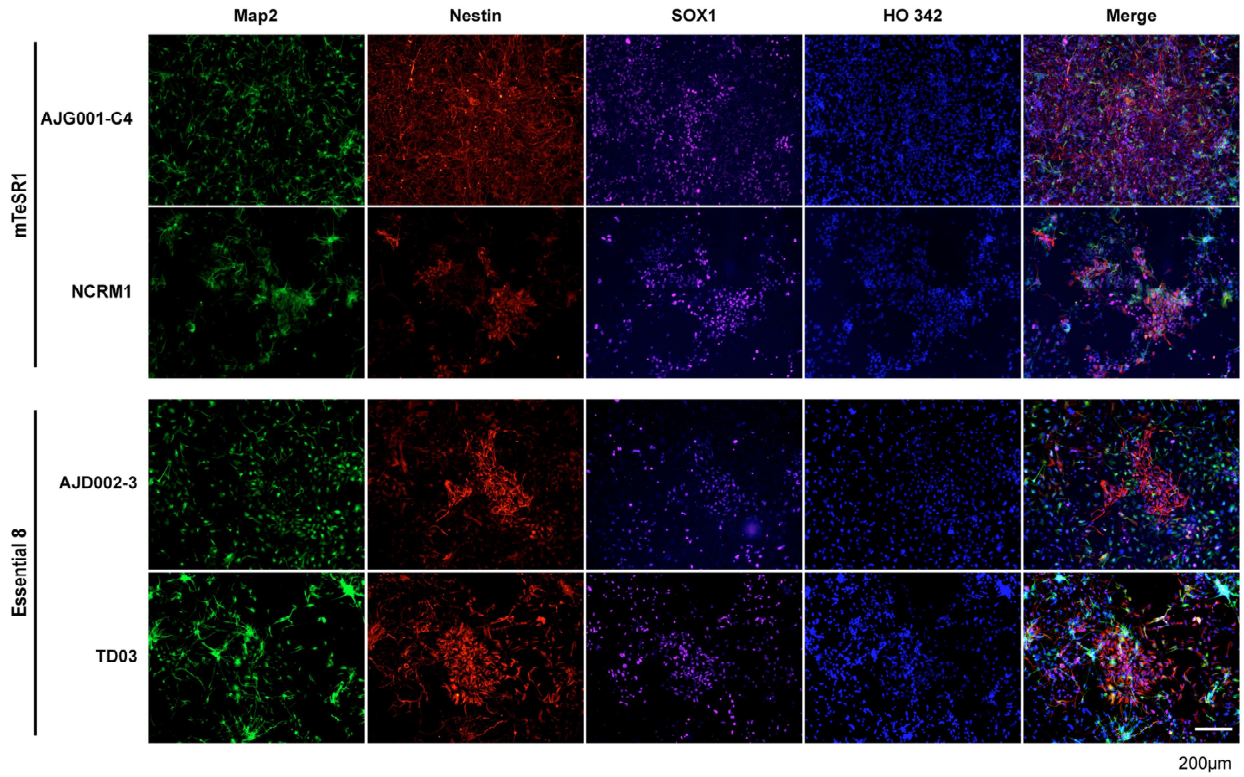

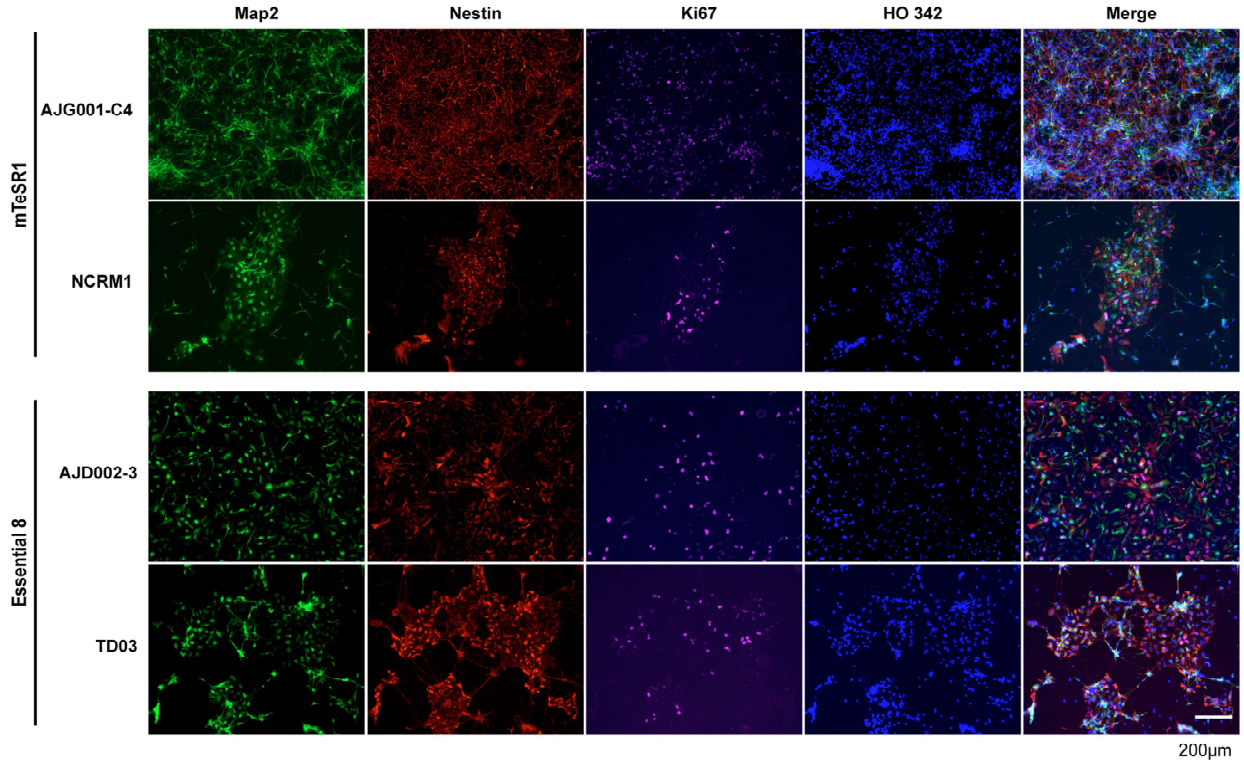

B

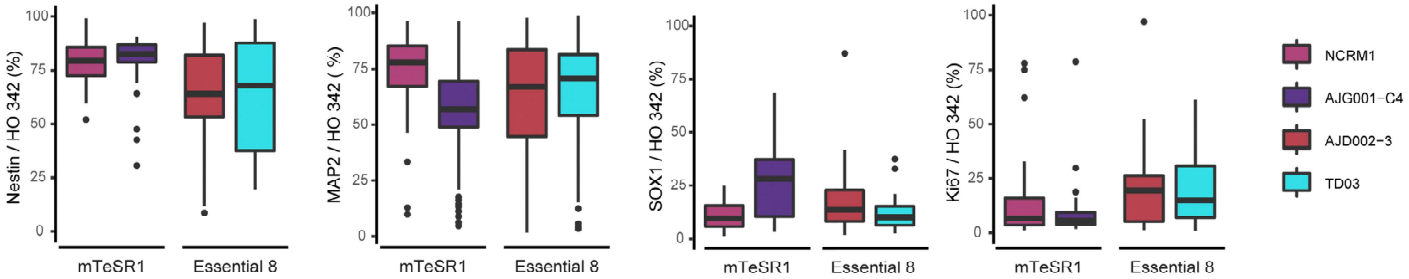

Chen et al, Supplementary Figure S3

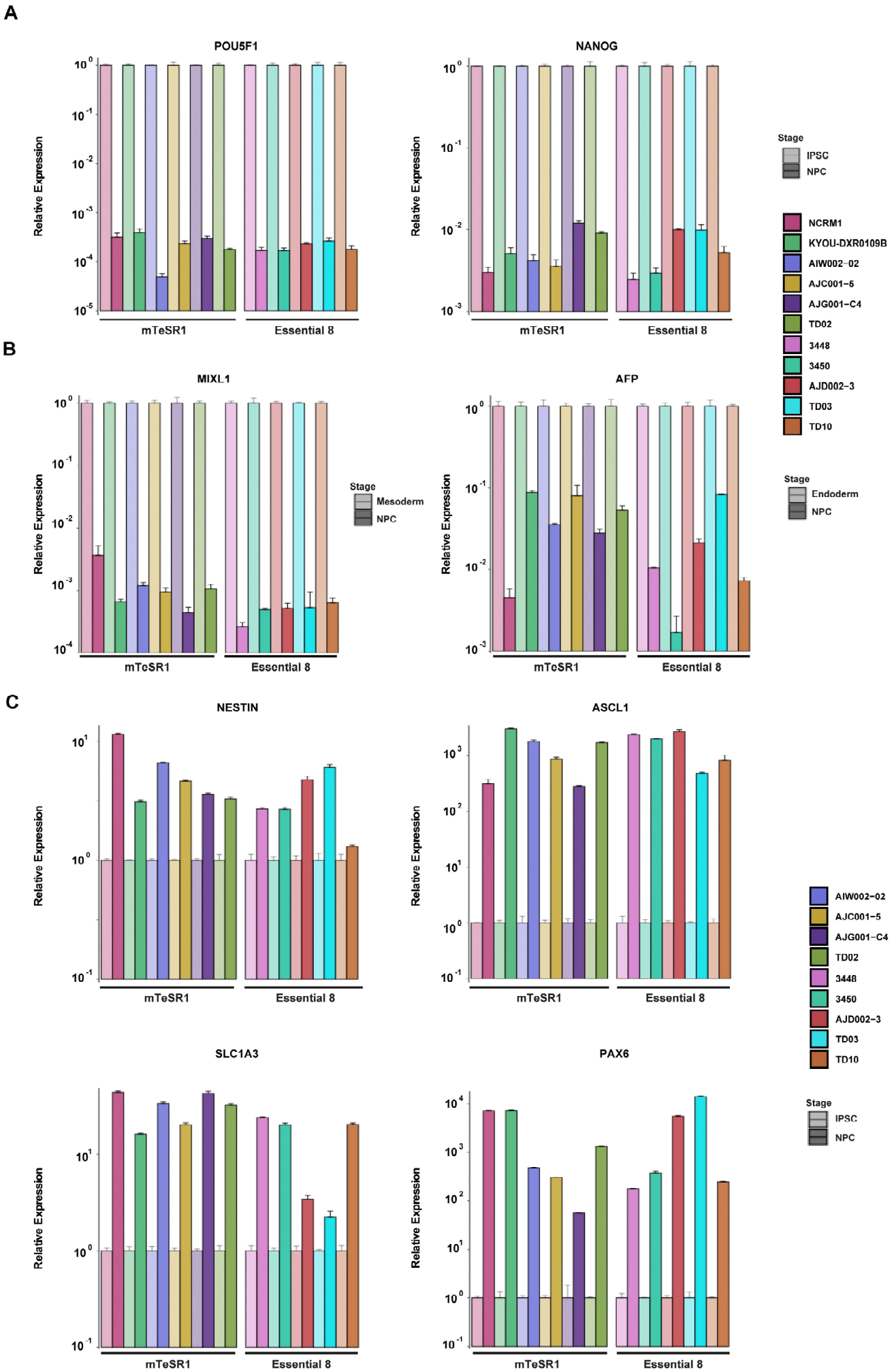

Chen et al, Supplementary Figure S4

A

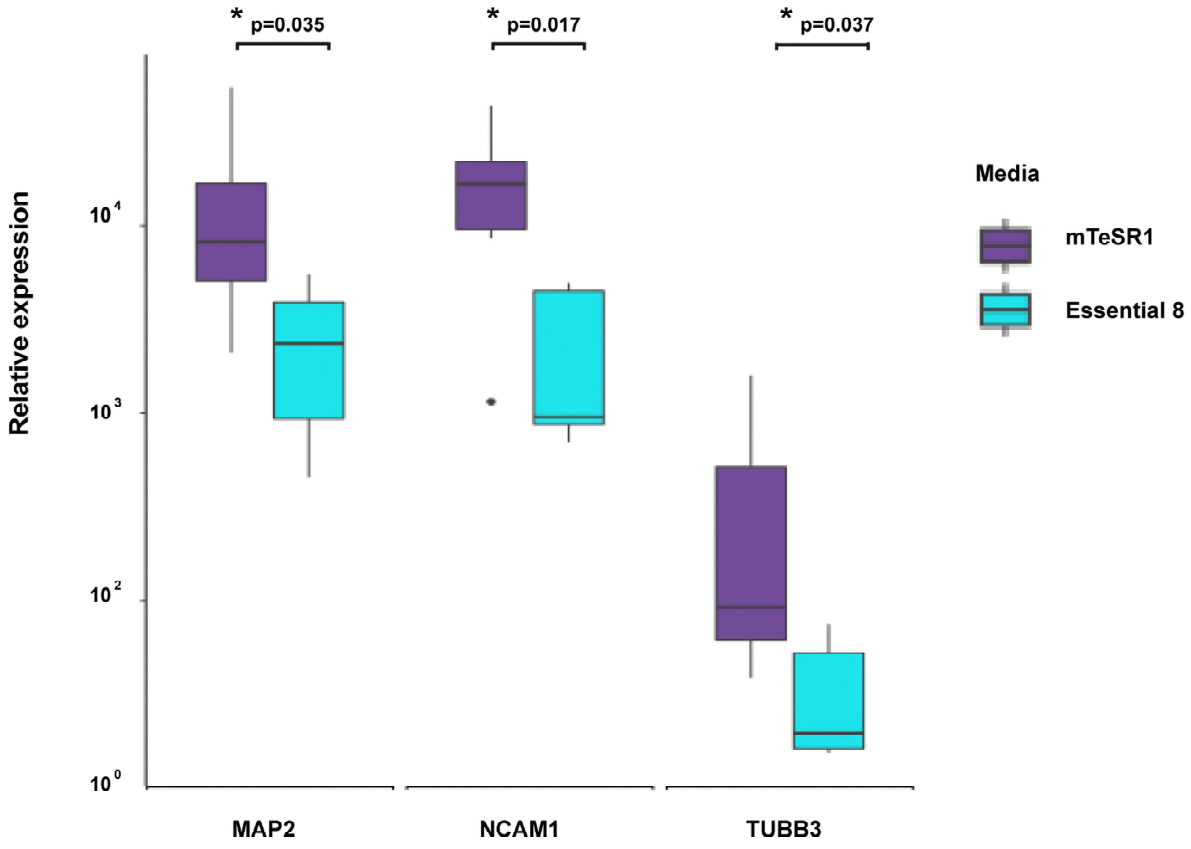

B

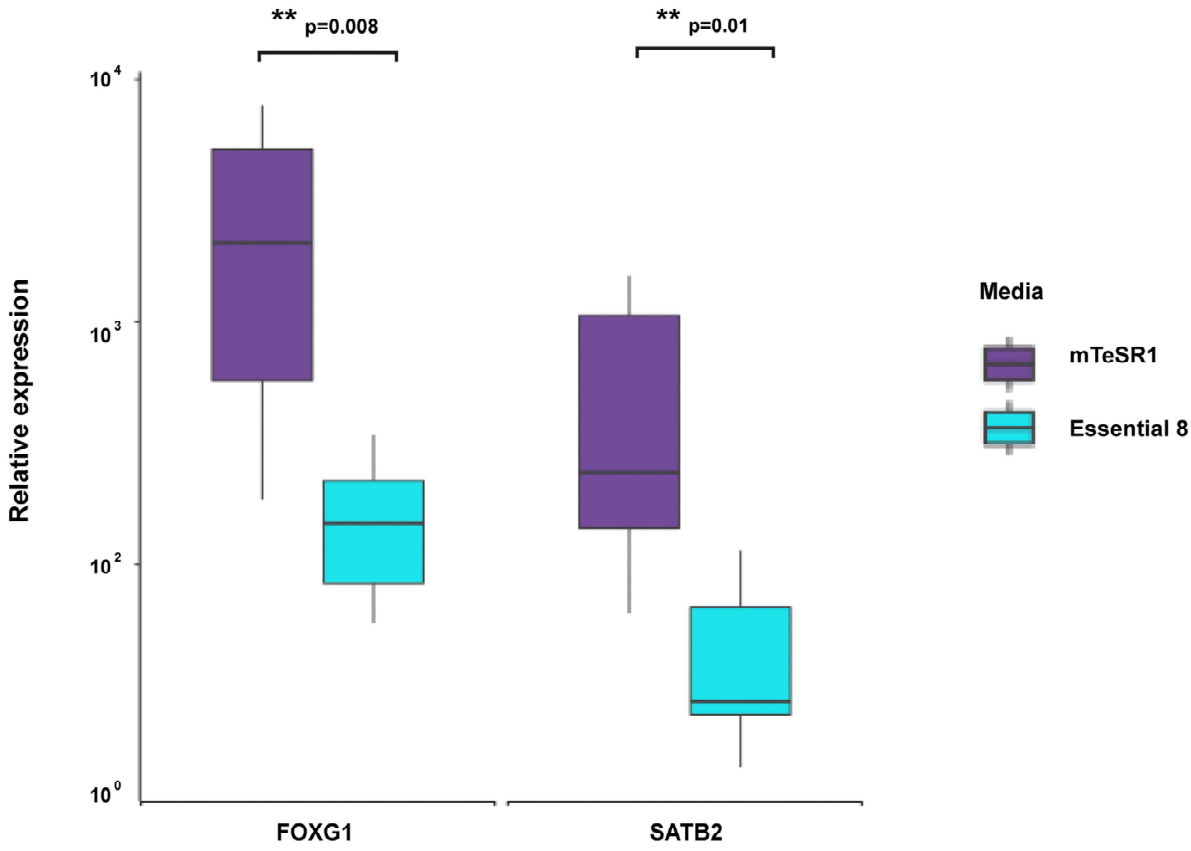

Chen et al, Supplementary Figure S5

Key resources table

REAGENT or RESOURCE	SOURCE	IDENTIFIER
Antibodies		
Rabbit polyclonal anti-Brn2/POU3F2	Cell Signaling	Cat#12137; RRID: AB_2797827
Mouse monoclonal anti-CD44	BD Biosciences	Cat#550392; RRID: AB_2074674
Mouse monoclonal anti-Ki-67	BD Biosciences	Cat#556003; RRID: AB_396287
Chicken polyclonal anti-MAP2	EnCor Biotechnology	Cat#CPCA-MAP2; RRID: AB_2138173
Rabbit polyclonal anti-Nanog	abcam	Cat#ab21624; RRID: AB_446437
Rabbit polyclonal anti-Nestin	abcam	Cat#ab92391; RRID: AB_10561437
Goat polyclonal anti-Oct-3/4(N-19)	Santa Cruz Biotechnology	Cat#sc-8628; RRID: AB_653551
Mouse monoclonal anti-PAX6	DSHB	Cat#AB_528427; RRID: AB_528427
Rabbit polyclonal anti-SMA1	abcam	Cat#ab5694; RRID: AB_2223021
Goat polyclonal anti-SOX1	R&D Systems	Cat#AF3369; RRID: AB_2239879
Rabbit polyclonal anti-SOX9	Millipore	Cat#AB5535; RRID: AB_2239761
Mouse monoclonal anti-SSEA-4(813-70)	Santa Cruz Biotechnology	Cat#sc-21704; RRID: AB_628289
Rabbit monoclonal anti-TBR1	abcam	Cat#ab31940; RRID: AB_2200219
Mouse monoclonal anti-TRA-1-60R	Stemcell Technologies	Cat#60064; RRID: AB_2686905
Rabbit monoclonal anti-Vimentin	Abcam	Cat#ab92547; RRID: AB_10562134
Mouse monoclonal anti-Tubulin- βIII	Millipore	Cat#MAB5564; RRID: AB_11212768
Hoechst 33342	ThermoFisher Scientific	H3570

Primers used in q-PCR experiments			
Gene ID	**Gene Name**	**Accession number**	**Assay ID**
ACTB	Actin, beta	NM_001101.3	Hs01060665_g1
AFP	Alpha fetoprotein	NM_001134.2	Hs01040598_m1
ASCL1	Achaete-scute family bHLH transcription factor 1	NM_004316.3	Hs00269932_m1
MYC	v-myc avian myelocytomatosis viral oncogene homolog	NM_002467.4	Hs00153408_m1
GAPDH	Glyceraldehyde-3-phosphate dehydrogenase	NM_001256788.2	Hs02786624_g1
KLF4	Kruppel like factor 4	NM_001314052.1	Hs00358836_m1
MAP2	Microtubule associated protein 2	NM_001039538.1	Hs00258900_m1
MIXL1	Mix paired-like homeobox	NM_031944.2	Hs00430824_g1
NANOG	NANOG homeobox	NM_001297698.1	Hs02387400_g1
NCAM1	Neural cell adhesion molecule 1	NM_000615.6	Hs00941830_m1
NES	Nestin	NM_006617.1	Hs04187831_g1
PAX6	Paired box 6	NM_000280.4	Hs01088114_m1
POU5F1 (OCT3/4)	POU class 5 homeobox 1	NM_001173531.2	Hs04260367_gH
SLC1A3	Solute carrier family 1 member 3	NM_001166695.2	Hs00904823_g1
SOX2	SRY-box 2	NM_003106.3	Hs04234836_s1
TUBB3	Tubulin beta 3 class III	NM_001197181.1	Hs00801390_s1
VIM	Vimentin	NM_003380.3	Hs00958111_m1
ZFP42	ZFP42 zinc finger protein	NM_001304358.1	Hs00399279_m1

Table S3. Quantification of pluripotency gene expression in hiPSCs by q-PCR analysis (mean ± SEM of relative gene expression, normalized to GAPDH and ACTIN)

Cell line	OCT3/4	SOX2	NANOG	c-MYC	ZFP42	KLF4
H9	2.219±0.310	0.1400±0.0065	0.0657±0.0044	0.0420±0.0044	0.0524±0.0048	0.000157±0.000037
NCRM1	1.614±0.135	0.6026±0.0105	0.3019±0.0012	0.0661±0.0034	0.2360±0.0015	0.000042±0.000009
KYOU-DXR0109B	1.168±0.108	0.5223±0.0061	0.1148±0.0008	0.0998±0.0013	0.1403±0.0023	0.000082±0.000014
AIW002-02	3.567±0.298	0.1226±0.0129	0.0748±0.0025	0.0298±0.0040	0.0737±0.0027	0.000101±0.000017
AJC001-5	2.194±0.383	0.1540±0.0081	0.0525±0.0036	0.0513±0.0017	0.0491±0.0035	0.000224±0.000008
AJG001-C4	1.763±0.096	0.2163±0.0087	0.0332±0.0016	0.0310±0.0029	0.0287±0.0024	0.000116±0.000011
TD02	2.199±0.263	0.1753±0.0170	0.0458±0.0062	0.0483±0.0036	0.0316±0.0024	0.000162±0.000025
3448	2.248±0.144	0.1515±0.0045	0.0446±0.0014	0.0615±0.0024	0.0552±0.0041	0.000113±0.000011
3450	2.633±0.345	0.1475±0.0053	0.0554±0.0061	0.0883±0.0042	0.0574±0.0026	0.000183±0.000009
AJD002-3	2.036±0.209	0.1556±0.0080	0.0499±0.0032	0.0545±0.0027	0.0405±0.0028	0.000181±0.000025
TD03	2.626±0.406	0.1267±0.0208	0.0616±0.0089	0.0689±0.0054	0.0440±0.0050	0.000217±0.000002
TD10	1.771±0.274	0.1128±0.0057	0.0484±0.0025	0.0420±0.0015	0.0404±0.0032	0.000158±0.000024
TD22	4.221±0.688	0.1991±0.0066	0.0641±0.0023	0.0482±0.0016	0.0378±0.0027	0.000206±0.000022